Extended Methods:

Patient consent and cohort

Tumor tissue acquisition was performed under an Institutional Review Board (IRB) protocol approved at UT Southwestern Medical Center. Informed written consent was obtained from all patients in accordance with institutional and NIH/NCI regulations. Tumor tissue was triaged for snap freezing, histology, and models generation. For model generation, fresh tumor tissue was placed in sterile 15 ml falcon tubes in RPMI-1640 media containing gentamycin and 1% Penicillin-Streptomycin and transported on wet ice. Primary cell line isolation and PDX generation were initiated within two hours of resection.

Establishing cell lines from patient tumor tissue and PDX models

Cell lines were developed from patient tumor tissue or PDX models using the same protocol. Tumor tissue was minced with twin sterile razor blades until it had the consistency of a smooth paste. Tissue was re-suspended in 10 ml of sterile tissue culture trypsin (0.05%, 0.53 mM EDTA; Corning) in a 15 ml Falcon tube and incubated for 30 minutes at 37°C with agitation to dissociate the tumor tissue from collagenous stroma. Undigested tissue (sediment) and tumor cell aggregates (supernatant) were separated by gravity. The undigested tissue was serially exposed to trypsin for 6x30 minute cycles of trypsin digestion. The tumor cell aggregates recovered were added to 1 ml of fetal bovine serum (FBS) to neutralize the trypsin and concentrated by centrifugation at 2,000 RPM for 2 minutes. The tumor cell aggregates were then re-suspended in growth media consisting of Keratinocyte-SFM (Life Technologies) supplemented with prequalified recombinant Epidermal Growth Factor and Bovine Pituitary Extract (Life Technologies), 2% FBS (Sigma), and 1% antibiotic-antimycotic (Life Technologies). The cells were cultured on plates pre-coated with collagen solution. Collagen solution was of rat-tail type I collagen (Millipore) at a final concentration of 50 µg/ml in 10 mM acetic acid. Plates coated with collagen were allowed to incubate for several minutes and subsequently washed

with complete media prior to cell seeding. Cells were incubated at 37°C with 5% CO_2. Tumor cells on the plates were readily apparent by morphology relative to stromal elements (e.g. fibroblasts). Contaminating stromal cells were removed by differential trypsinization or selective scraping of the plates as necessary. Cell lines were routinely evaluated for the absence of mycoplasma contamination by DAPI staining. This isolation method was compared against the method of conditionally reprogrammed cells (1) and was found to be superior for the time required for derivation of the cell line and the ability to isolate pure tumor cell populations (n=3). That finding is consistent with a recent study, in which conditionally reprogrammed culture was not effective in supporting growth of primary ovarian cell lines (2). We also used an established protocol for organoid development (3) followed by plating on collagen coated plates. We did not observe an additional benefit of this approach on the cases tested (n=2), although it did yield cell lines comparable to the optimized approach (not shown). The development of pure cell lines required 8-12 weeks on average. Instances where we failed to develop cell lines were due to lack of sufficient tumor tissue, overgrowth by stromal cells, contamination or a very slow tumor cell growth.

Establishing patient derived xenografts

NOD-SCID IL2Rγ null (NSG) mice were maintained in a barrier facility under HEPA-filtered air with food and water available as desired. Food, water and cage bedding were sterilized prior to use. Animal experiments fulfilled National Institutes of Health and UT Southwestern requirements for humane animal care and all procedures were approved by the UT Southwestern Institutional Animal Care and Use Committee. NSG mice were anesthetized with isoflurane and, once sedated, subjected to survival surgery. For subcutaneous patient derived xenograft (PDX) generation, the mouse flank was shaved and cleansed with 70% alcohol and Betadine. A 0.5-1 cm incision was made through the skin and subcutaneous tissue. A tumor fragment (approximately 1x3 mm) was then implanted into the flank and the incision was closed

with 4-0 Vicryl suture. For orthotopic PDX, a small incision was made through the abdominal wall and peritoneum. The tail of the pancreas was gently extruded with blunt forceps, and a tumor fragment (approximately 1x3 mm) was sutured to the pancreas using 6-0 sterile silk black braided suture. The tail of the pancreas was then placed back inside the peritoneal cavity, and incision site was closed in two layers: 1st peritoneum with 6-0 silk sterile suture, and 2nd skin with 6-0 braided sterile silk suture. Mice were provided with buprenorphine as an analgesic and monitored daily for two consecutive days after surgery with particular attention paid to animal distress, wound dehiscence, and signs of infections. Thereafter, they were examined 2-3 times per week. Monitoring for tumor growth was performed up to nine months post implantation. Tumor size was assessed by measurement with calipers once a week. Tumor volume was approximated using measurements of tumor length and width using the formula: (length × (width2))/2. The mice were euthanized by CO_2 inhalation, and tumors were harvested once they reached volume ~1500mm^3. PDX tumor tissue was divided for: snap freezing, fixation in 10% buffered formalin for paraffin embedding/histology, cryopreservation, PDX cell line development and passaging.

Whole exome sequencing alignment and quality metrics

A total of 25 primary tumors/normal pairs, 56 primary and PDX cell lines and 54 PDX tumors were subjected to paired-end whole exome sequencing and run on Illumina HiSeq2500. The sequencing libraries were obtained using commercially available exome capture kits as per the manufacturer's protocol. The sequences were demultiplexed using CASAVA and FASTQ files were obtained. The sequences were aligned using BWA tool to the human genome (UCSC-hg19 build) and the aligned files were obtained in BAM format (4). Duplicates were removed using PICARD (http://broadinstitute.github.io/picard/), and reads with quality less than a phred score of 10 were filtered out. Picard HsMetrics was used to capture coverage and alignment

metrics for the BAM files. An average coverage of 120±34x was obtained across the cases/models with 94% of unique reads aligned and 94% of the targeted bases having at least 20x coverage. The exome sequencing data is deposited at dbGaP.

Somatic Mutation calling and post-filtering

Somatic point mutations and insertions/deletion in the sequenced tumors tissue/cell lines/PDXs were obtained using MuTect and VarScan, respectively with default settings, as we have previously reported (5). The tumor cases and models were compared against the respective normal tissue. The mutations were annotated using Oncotator tool from the Broad Institute. For known PDA mutations; KRAS, TP53 and SMAD4, MuTect cut-offs were relaxed to tumor reference count <=5 and IGV was used to confirm those mutations. Indels with reference allele counts greater than 8 and tumor variant allele counts greater than 3 were only considered. All mutations were subjected to a post-filtering mouse and paralog removal (MAPEX) algorithm where the sequences containing the mutations were Blast-filtered against both the human (GRCh37, hg19) and mouse (GRCm38, mm10) databases. Percent identity scores for the sequences were captured. Any read with 100% identity in mouse or percentage identity greater in mouse was considered as 'potential mouse read'; 100% identity in both human and mouse was considered a 'possible paralog' and was flagged as 'rejected' and given a score of 0. A somatic mutation was 'accepted' only when the aggregate score for all its sequences was > 50%. This rigorous post-filtering algorithm effectively removed all the potential mouse mutations and known paralogous calls.

Copy number analysis

GATK 'DepthOfCoverage' algorithm was used to obtain coverage across all the sequenced cases. ExomeCNV and DNAcopy packages in R/Bioconductor were used to obtain the log ratio between tumor and normal and to normalize the data by circular binary segmentation algorithm

to generate segment files. The copy number alteration per gene was then obtained using the GISTIC2 program (6). The joint segment size was set to 4 and the confidence level was set to 95%. The data were summarized and evaluated as we have previously published (5).

RNA sequencing analysis

PDA cell lines and PDX models were subjected to 50 bp paired-end RNA sequencing. The data were demultiplexed and the raw Fastq files were aligned to the human genome (UCSC-hg19 build) using TopHat2 (6) alignment algorithm to generate aligned BAM files. HTseq-count (7) algorithm was used to obtain the counts per gene for each sample. EdgeR (8) a Bioconductor/R package, was used to normalize and remove batch effects in the count data.

The analyses for the gene expression were carried out using standard Euclidean based clustering with clinical cases of defined subtypes (9). Alternatively, the top 200 genes with high variance in the cell lines were used to cluster with the PDXs based on Euclidean distance.

Phylogenetic Analysis

Phylogenetic tree reconstruction was performed similar to the algorithms defined in Gerlinger et al (10). Briefly, a binary matrix of mutations was constructed for the models. MEGA5 software was used to obtain the maximum parsimony tree using the subtree-pruning regrafting algorithm (11). The normal were used to root the phylogenetic trees. The trees were re-plotted using Adobe Illustrator keeping the branch lengths conserved.

Analysis of DNA/RNA sequencing data

Statistical analyses of exome and RNA sequencing were performed using packages in R statistical software. Correlations between PDA models were obtained using Spearman correlation method. Heatmaps and oncoprints were obtained using gplots and pheatmap

packages in R. Venn diagrams showing the number of mutations conserved among models were obtained using the VennDiagram package in R. Alleleic balance in the RNA sequencing data was determined by using IGV focused over mutational events identified by exome sequencing.

Tumor clonality and hierarchical sample clustering

Tumor cellularity and heterogeneity for both tumor and cell lines of samples EMC226, EMC519, and EMC114 was estimated using THetA2 to verify zygosity of clonal mutations. Variant allele frequencies (VAF) were then normalized by dividing called VAF by the highest reported VAF for a clonal homozygous mutation in each sample. We obtained TCGA sample VAF's from the TCGA website and normalized by dividing called VAF by the provided purity estimate. Hierarchical clustering of tumor, pdx, and cell line samples was performed using the function hclust [2] in R with method=average, with squared Euclidean distances computed on the presence/absence matrix of called mutations in each sample.

Tumorgenic potential of primary cell lines

Between 1-2x10^6 cells suspended in 50µl of Matrigel were injected into the pancreas of anesthetized NSG mice using incision and surgical closure techniques employed for orthotopic PDX generation. Mice were monitored for tumor growth as described above.

Immunohistochemistry:

Patient tumors and xenografts were fixed in 10% buffered formalin and processed for paraffin embedding. 5 µm sections were used for immunohistochemical stains on automated DAKO stainer as previously described (12). The primary mouse monoclonal anti-Ki67 (DAKO, pre-diluted, IR62661-2) was employed.

Western blotting, RPPA, RNAi transfection

Drugs used in the study were purchased from Selleck Chemical and diluted in DMSO as vehicle. Antibodies against GAPDH (SC-25778) were from Santa Cruz Biotechnology. Anti-p16INK4a (AF5779) was from R&D Systems, while the RB antibody (G3-235) was from BD. Cells were trypsinized and lysed in RIPA buffer (10% NP-40, 1% SDS, 5% sodium deoxycholate, 500 mM Tris-HCl pH 7.4, 1.5 M NaCl, 10 mM EDTA) containing protease inhibitor cocktail (Roche) and Pierce™ phosphatase inhibitor tablets for 1 hour on ice. Lysate was collected after centrifuging samples at 14,000 RPM for 20 minutes. Protein concentration was assessed using DC™ protein assay (Bio-Rad) according to the manufacturer's protocol. Absorbance and subsequent protein concentration was determined by a BIOTEK plate reader and Gen5 software. RNAi transfection and measurement of survival by cell-titer-glow was performed as previously described (13). The KRAS RNAi pool was from Dharmacon.

Immunofluorescence

Cells or tissues were fixed with methanol. For the detection of nuclear antigens extraction was performed with 1X PBS containing 0.5% Triton X-100 for 10 minutes. Staining was performed using primary antibodies diluted in PBS supplemented with 5% BSA and 0.4% NP-40. Fixed cells or tissues were then incubated with primary antibodies according to the vendor specifications for 30-60 minutes at room temperature. Anti-cytokeratin 8 was from Invitrogen, anti-vimentin was from Cell Signaling, and anti-p53 was from Santa Cruz. Cells were washed with 1X PBS and incubated with fluorescent conjugated secondary antibodies (Alexa Fluor® 488 goat anti-rabbit IgG 1:500; Life Technologies, and Rhodamine anti-mouse IgG 1:500; Life Technologies) and counterstained with Hoechst (1:250; Life Technologies) for 30 minutes at room temperature. Images were taken at 40X magnification and edited using ImageJ software.

Flow cytometry

Cells were incubated with fresh media containing 1:100 BrdU labeling solution (Invitrogen) for 90 minutes. Trypsin was then added and cells washed with PBS following BrdU incubation. Cells were fixed with 70% ethanol for 1 hour at 4°C. Samples were incubated with 2M HCl containing 0.3 mg/ml pepsin solution for 30 minutes. Acid was neutralized with 0.1M sodium tetraborate pH 8.5 and cells washed twice with IFA buffer (10mM HEPES pH 7.4, 25 mM NaCl, 4% FBS). Samples were incubated with FITC labeled anti-BrdU solution (1:50; BD Pharmingen™) for 30 minutes at room temperature. Samples were washed with IFA buffer and resuspended in PBS containing propidium iodide (20 µg/ml) and RNase (4 µg/ml) and allowed to incubate for 20 minutes in the dark. Cell cycle was assessed using a FACSCalibur flow cytometer and data analysis conducted on FloJo software.

Drug Sensitivity Analysis: The cell models were drug screened with a compound library of 305 agents as we have recently described in detail(14). Area under the curve (AUC) values for single-drug responses were z-score normalized. Subtype groups defined by the gene expression signature found in Collisson et al. were compared using a two-tailed, heteroscedastic t-test. Drugs that had significantly different sensitivities ($p<0.05$) between the quasi-mesenchymal group and the other subtypes were then clustered within both subtype groups using unsupervised hierarchal clustering methods in R. These subtype clusters were assembled into a single heatmap for comparison.

REFERENCES:

1. Liu X, Ory V, Chapman S, Yuan H, Albanese C, Kallakury B, et al. ROCK inhibitor and feeder cells induce the conditional reprogramming of epithelial cells. Am J Pathol. 2012;180:599-607.
2. Ince TA, Sousa AD, Jones MA, Harrell JC, Agoston ES, Krohn M, et al. Characterization of twenty-five ovarian tumour cell lines that phenocopy primary tumours. Nature communications. 2015;6:7419.
3. Boj SF, Hwang CI, Baker LA, Chio, II, Engle DD, Corbo V, et al. Organoid models of human and mouse ductal pancreatic cancer. Cell. 2015;160:324-38.
4. Li H, Durbin R. Fast and accurate short read alignment with Burrows-Wheeler transform. Bioinformatics. 2009;25:1754-60.

5. Witkiewicz AK, McMillan EA, Balaji U, Baek G, Lin WC, Mansour J, et al. Whole-exome sequencing of pancreatic cancer defines genetic diversity and therapeutic targets. Nature communications. 2015;6:6744.
6. Kim D, Pertea G, Trapnell C, Pimentel H, Kelley R, Salzberg SL. TopHat2: accurate alignment of transcriptomes in the presence of insertions, deletions and gene fusions. Genome Biol. 2013;14:R36.
7. Anders S, Pyl PT, Huber W. HTSeq--a Python framework to work with high-throughput sequencing data. Bioinformatics. 2015;31:166-9.
8. Robinson MD, McCarthy DJ, Smyth GK. edgeR: a Bioconductor package for differential expression analysis of digital gene expression data. Bioinformatics. 2010;26:139-40.
9. Collisson EA, Sadanandam A, Olson P, Gibb WJ, Truitt M, Gu S, et al. Subtypes of pancreatic ductal adenocarcinoma and their differing responses to therapy. Nature medicine. 2011;17:500-3.
10. Gerlinger M, Horswell S, Larkin J, Rowan AJ, Salm MP, Varela I, et al. Genomic architecture and evolution of clear cell renal cell carcinomas defined by multiregion sequencing. Nature genetics. 2014;46:225-33.
11. Tamura K, Peterson D, Peterson N, Stecher G, Nei M, Kumar S. MEGA5: molecular evolutionary genetics analysis using maximum likelihood, evolutionary distance, and maximum parsimony methods. Molecular biology and evolution. 2011;28:2731-9.
12. Witkiewicz AK, Borja NA, Franco J, Brody JR, Yeo CJ, Mansour J, et al. Selective impact of CDK4/6 suppression on patient-derived models of pancreatic cancer. Oncotarget. 2015;6:15788-801.
13. Franco J, Balaji U, Freinkman E, Witkiewicz AK, Knudsen ES. Metabolic Reprogramming of Pancreatic Cancer Mediated by CDK4/6 Inhibition Elicits Unique Vulnerabilities. Cell reports. 2016.
14. Witkiewicz AK, Balaji U, Eslinger C, McMillan E, Conway W, Posner B, et al. Integrated Patient-Derived Models Delineate Individualized Therapeutic Vulnerabilities of Pancreatic Cancer. Cell reports. 2016;16:2017-31.

Supplemental Figure Legends:

Figure S1. (A) Summary of the cases and abbreviated clinical pathological information. (B) Summary of copy number alterations in the sequenced tumor cohort as determined by GISTIC analysis, the positions of CDKN2A and SMAD4 deletions are indicated. (C) The copy number alterations defined in the present sequencing cohort (green) were subjected to unsupervised clustering with a previously published cohort of 109 cases (blue). (D) Oncoprints of core signaling pathways disrupted in the sequenced cohort. Blue denotes homozygous deletion, red denotes amplification, orange denotes tumor specific INDEL and green indicates tumor specific SNV. (E) Overall distribution of genetic events targeting oncogenic pathways in a previously published cohort of 109 cases.

Figure S2. (A) Summary of the cell lines and PDX models developed for each case. (B) Representative phase contrast images of cell lines derived from independent PDAC clinical cases (designated as case identifier "_C") and/or PDX models (designated as PDX identifier "_C"). Scale bar is 400 μm (C) Representative immunofluorescence staining of CK8 and vimentin for cell lines developed. Scale bar is 400 μm. Summary of staining is provided in the table. Staining was repeated on selected late passage models that retained the expression of CK8. (D) Representative images of CK8 and p53 immunofluorescence staining. Summary of p53 staining relative to the TP53 mutation in the primary tumor is shown in the table. (E) Pedigree charts of PDX development. The derivation of cell lines and exome sequencing of the models are

indicated by the legend. (E) Representative hematoxylin and eosin stained sections of the primary tumor and PDX tissue from three passages. Scale bar is 100 μm.

Figure S3. (A) Table summarizes the classification of the indicated models using the = Collisson et al. classifier. (B) Venn diagrams summarize the overlap in SNVs between the representative primary tumors and indicated cell lines. Allele frequency plots summarize the conservation of high frequency genetic events between the primary tumor and cell lines. Green bars denote genes in common. Fuchsia, red, and blue bars denote SMAD4, KRAS and TP53 mutations, respectively. Gray bars are unique to either the tumor or the cell line. (C) Specific integrated genome view analysis of variants that were not called by MuTect. The variants in these cases were not called due to strand bias or low reads in the specific region. (D) Heatmap of the Spearman correlation of all SNV events in the primary tumor and indicated cell line models. (E) Venn diagram, allele frequency plots and Spearman correlation of somatic single nucleotide variants from the indicated comparisons of primary tumor with various PDX within same passage, metastatic deposits and PDX derived cell lines. (F) The EMC1229 case was very challenging to sequence due to distinct histological features of the primary tumor. This resulted in overall low tumor-specific allele frequencies, which likely underlie the larger discordance between this case and the resultant models.

Figure S4.

(A) Summary of the number of genes that are common or unique to the tumor vs. PDX. (B) Mutant allele frequencies plots from the primary tumor and PDX. Common genes

are shown in green and unique genes are depicted in gray. Color bar highlights specific cancer associated genes as indicated. The Y-axis is the allele frequency of the mutation in the model, the X-axis is the allele frequency of mutation in the patient tumor. (C) Summary of the number of genes that are common or unique to the tumor vs. cell lines. (D) Mutant allele frequencies plots from the primary tumor and indicated cell lines. Common genes are shown in green and unique genes are depicted in gray. Color bar highlights specific cancer associated genes as indicated. The Y-axis is the allele frequency of the mutation in the model, the X-axis is the allele frequency of mutation in the patient tumor.

Figure S5

Gene ontology analysis of all unique variants identified was performed. This revealed an over-representation of events that target transcription or cell differentiation pathways. The p-value and gene names are provided.

Figure S6

(A) Summary of drugs that are selective for established cell lines vs. quasi-mesenchymal (QM) primary cell lines vs. other subtypes primary cell lines. P-value and number of events are shown. (B) Representative drugs that exhibit selectivity for established cell lines (MiaPaca2, Panc1, PL45, PL5, Capan2, Capan1, Hs766t, BxPC3, ASPC1) vs. primary cell lines of either QM or other subtypes ***denotes $p<0.001$ for the combined cell line models across the doses.

A.

Case	Diagnosis	Vital status	Overall survival (days)
EMC1012_T	PDA, no special type	Alive	78
EMC1022_T	PDA, no special type	Alive	68
EMC114_T	PDA, no special type	Alive	237
EMC119_T	PDA, no special type	Alive	50
EMC1222_T	PDA, no special type	Alive	301
EMC1229_T	PDA, no special type	Alive	294
EMC129_T	PDA, no special type	Alive	273
EMC18128_T	Sarcomatoid/anaplastic carcinoma	DOD	92
EMC2095_T	PDA, no special type	DOD	368
EMC226_T	PDA, no special type	Alive	232
EMC26_T	Adenosquamous carcinoma	Alive	251
EMC29_T	PDA, no special type	Alive	248
EMC319_T	PDA, no special type	Alive	285
EMC3226_T	PDA, no special type	DOD	127
EMC35_T	PDA arising from IPMN	DOD	166
EMC41_T	PDA, no special type	Alive	363
EMC43_T	PDA, no special type	Alive	201
EMC514_T	PDA, no special type	Alive	271
EMC519_T	PDA, no special type	Alive	149
EMC528_T	PDA, no special type	Alive	216
EMC62_T	PDA, no special type	Alive	140
EMC7310_T	Adenosquamous carcinoma	DOD	128
EMC810_T	PDA, no special type	Alive	135
EMC827_T	PDA arising from IPMN	Alive	118
EMC828_T	PDA, no special type	DOD	365
EMC93_T	PDA arising from IPMN	Alive	376
EMCT2_T	PDA, no special type	DOD	797

B.

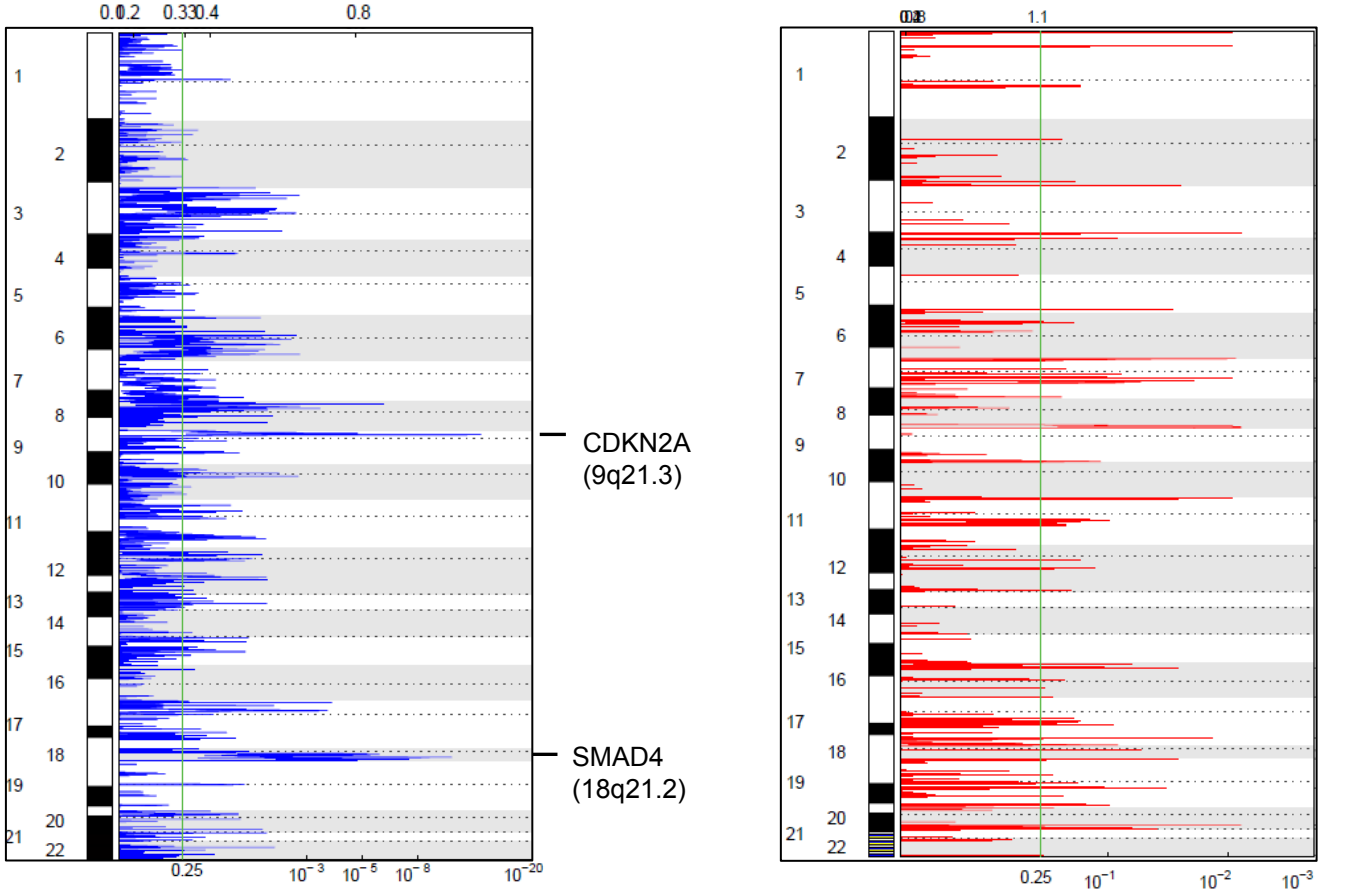
CDKN2A
(9q21.3)
SMAD4
(18q21.2)

C.

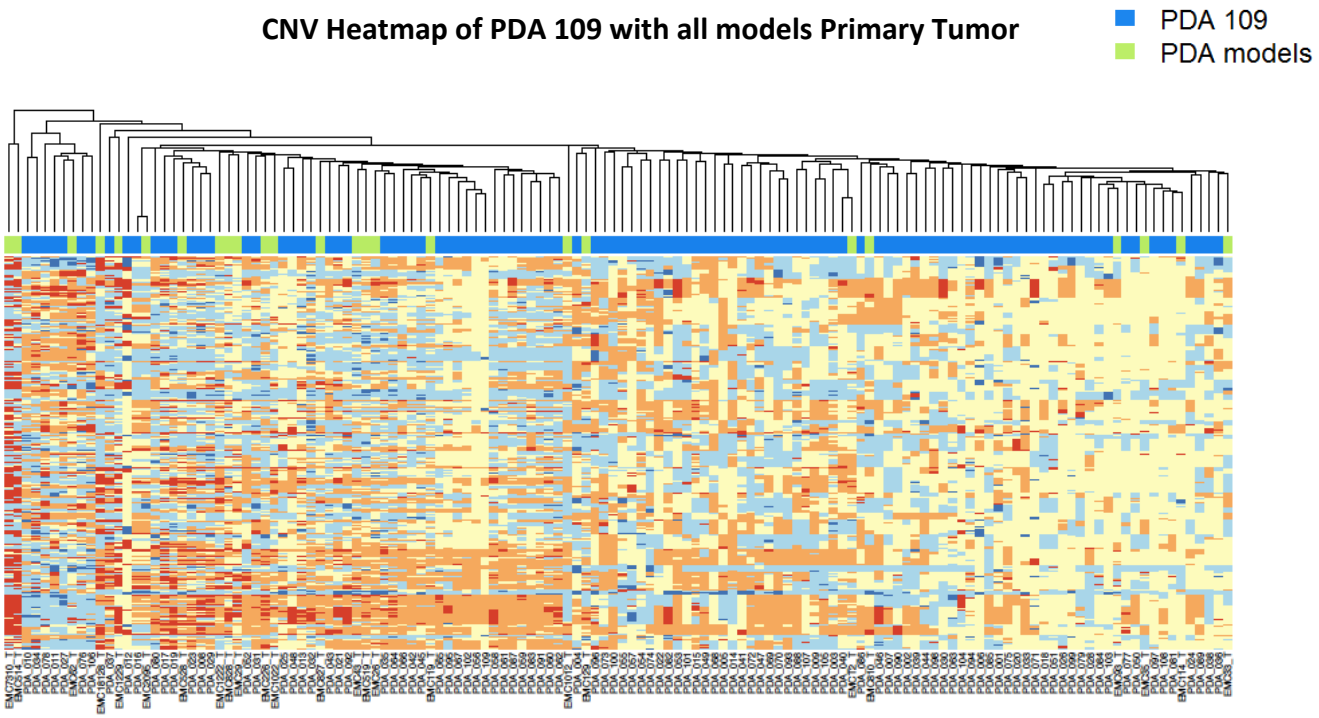
CNV Heatmap of PDA 109 with all models Primary Tumor
PDA 109
PDA models

D.

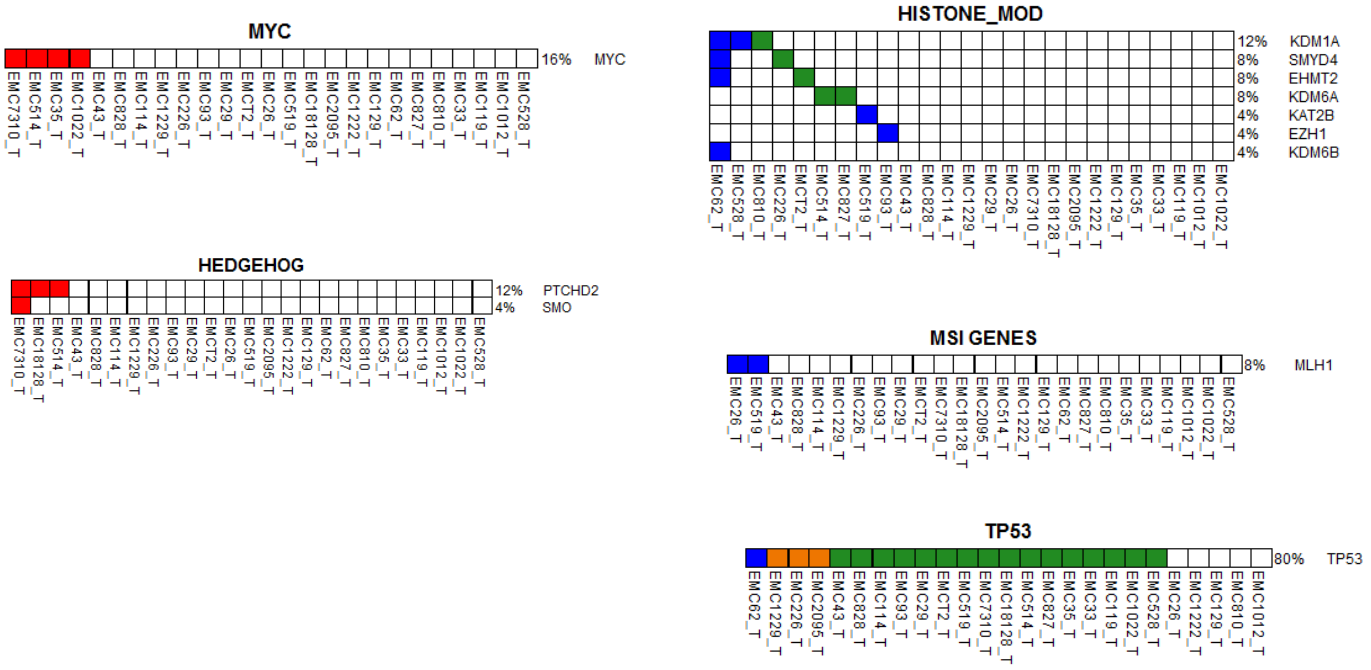
MYC
16% MYC
HISTONE_MOD
12% KDM1A
8% SMYD4
8% EHMT2
8% KDM6A
4% KAT2B
4% EZH1
4% KDM6B
HEDGEHOG
12% PTCHD2
4% SMO
MSI GENES
8% MLH1
TP53
80% TP53

E.

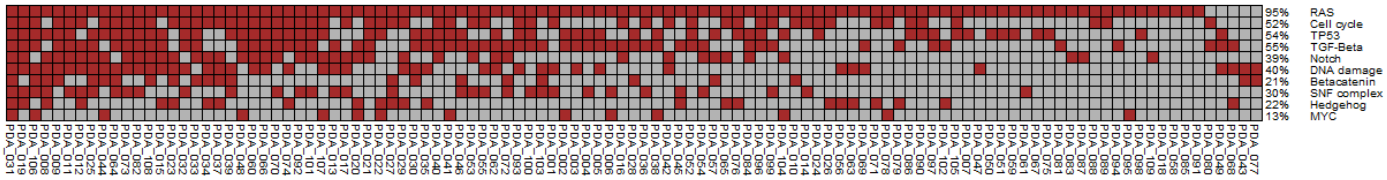
95% RAS
52% Cell cycle
64% TP53
55% TGF-Beta
39% Notch
40% DNA damage
21% Betacatenin
30% SNF complex
22% Hedgehog
13% MYC

A.

Case	Cell Line	PDX
EMC1022_T	X	X
EMC114_T	X	X
EMC119_T	X	X
EMC1222_T	X	X
EMC1229_T	X	X
EMC129_T	X	X
EMC18128_T	X	X
EMC226_T	X	X
EMC26_T	X	X
EMC29_T	X	X
EMC3226_T	X	X
EMC41_T	X	X
EMC43_T	X	X
EMC519_T	X	X
EMC810_T	X	X
EMC827_T	X	X
EMC828_T	X	X
EMCT2_T	X	X
EMC2095_T	X	
EMC514_T	X	
EMC7310_T	X	
EMC1012_T		X
EMC319_T		X
EMC33_T		X
EMC35_T		X
EMC528_T		X
EMC62_T		X
EMC93_T		X

B.

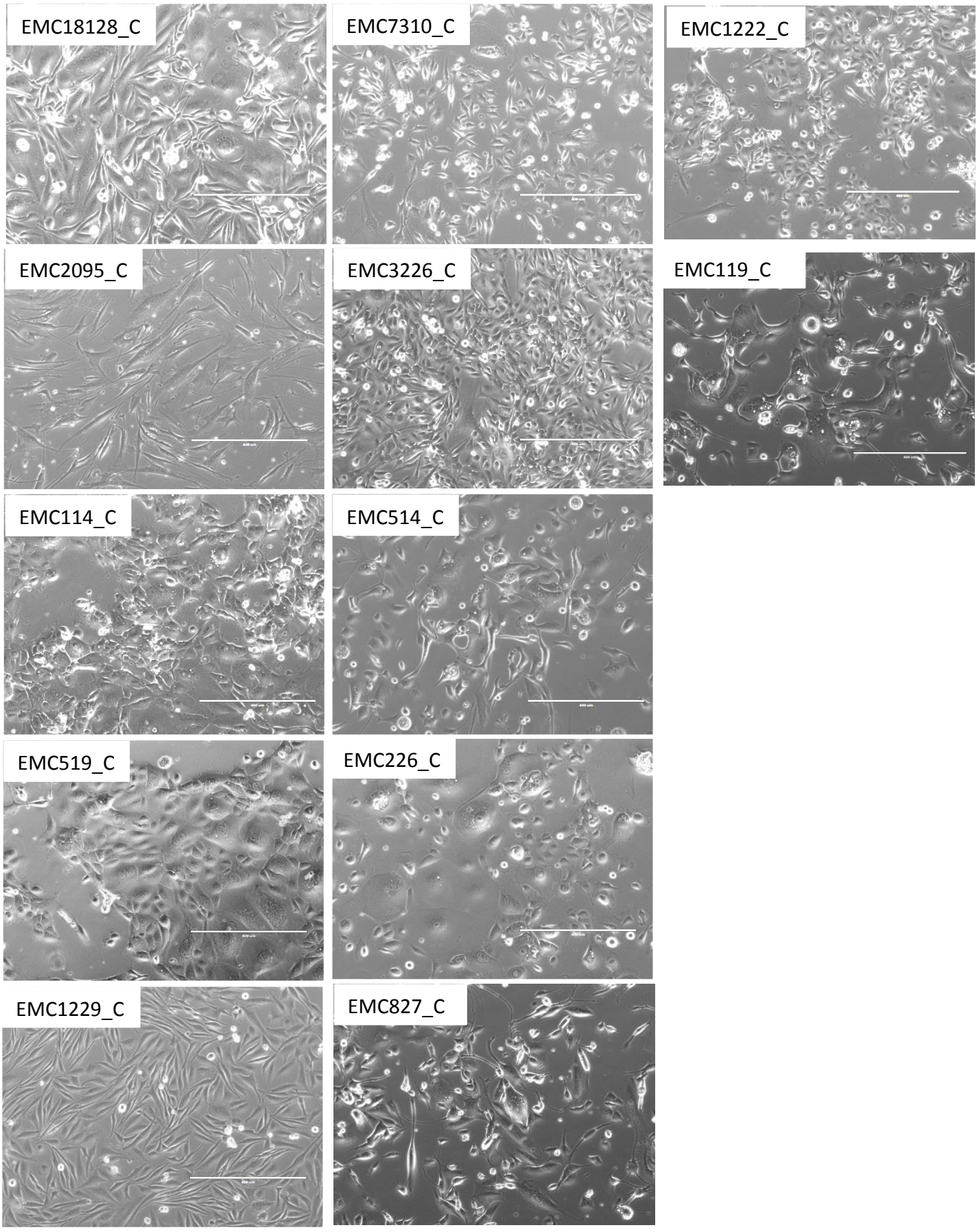
EMC18128_C
EMC7310_C
EMC1222_C
EMC2095_C
EMC3226_C
EMC119_C
EMC114_C
EMC514_C
EMC519_C
EMC226_C
EMC1229_C
EMC827_C

EMC1222_C

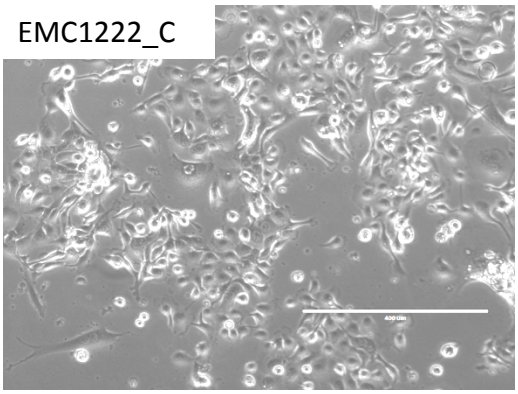

EMC1222x3b5_C

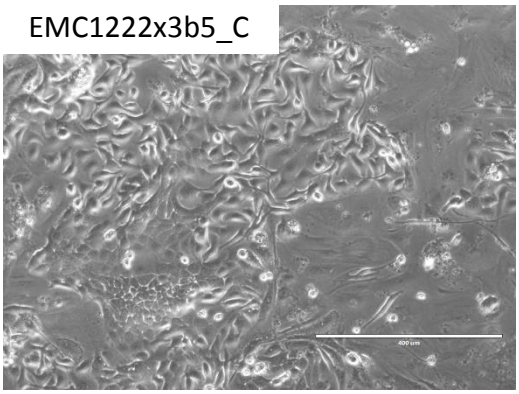

EMC1222x1b1_C

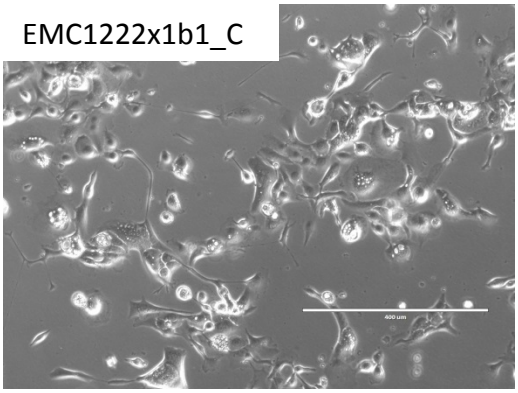

EMC1222x1a3_C

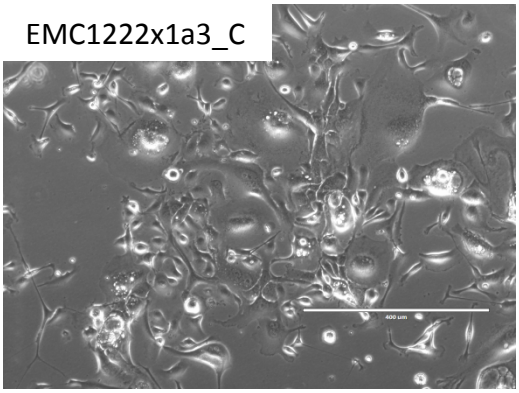

EMC1222o2a2_C2

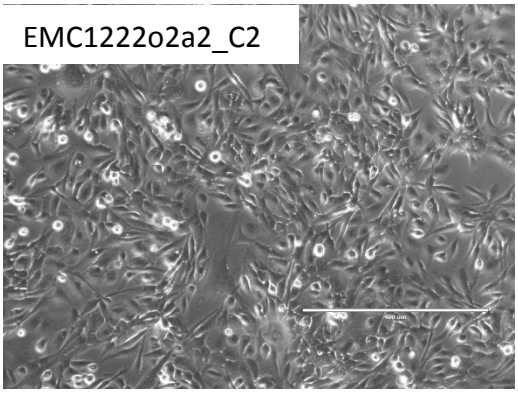

EMC1222x3c2_C

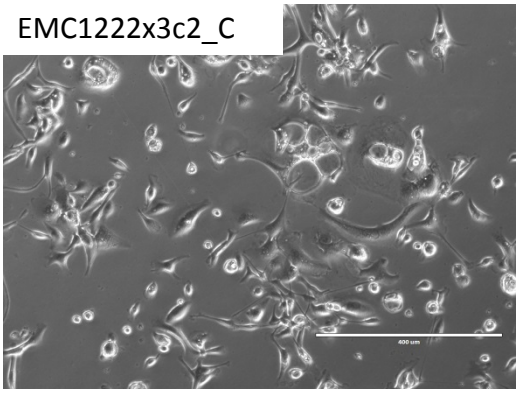

EMC226_C

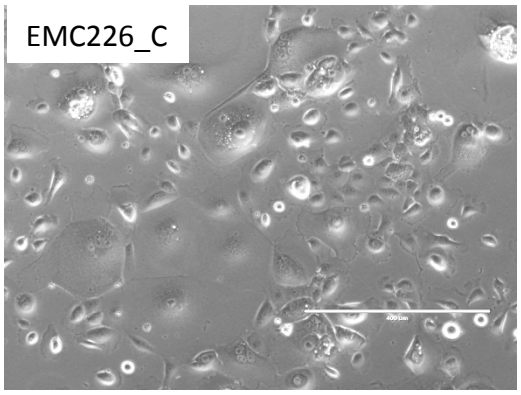

EMC226o1a5omMet_C

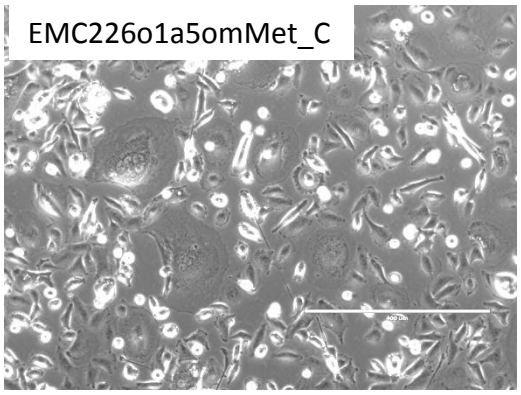

EMC226x1a1_C

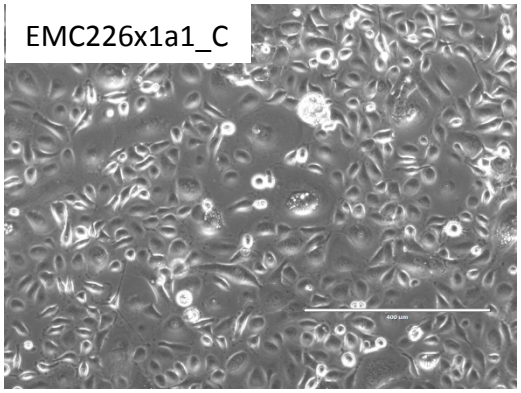

EMC226o1a5_C

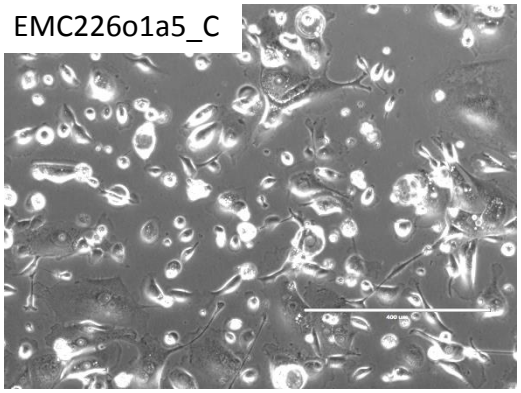

EMC226x2a2_C

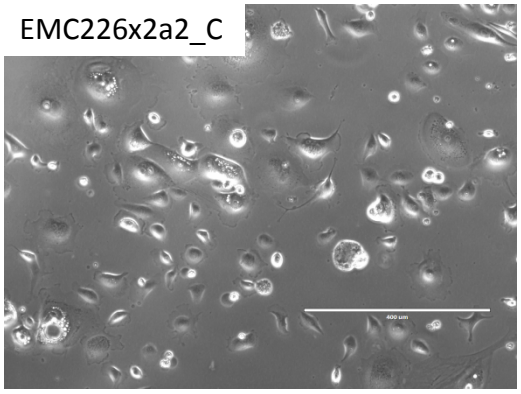

EMC828x1b1_C

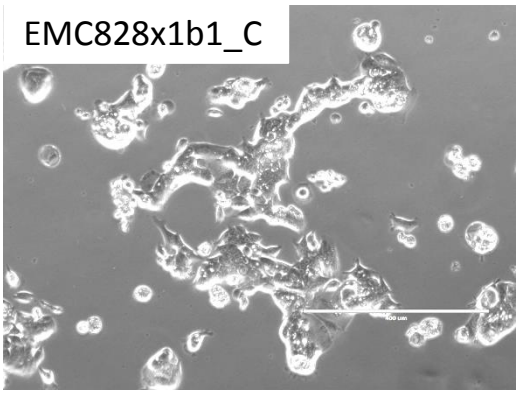

EMC828x1b3_C

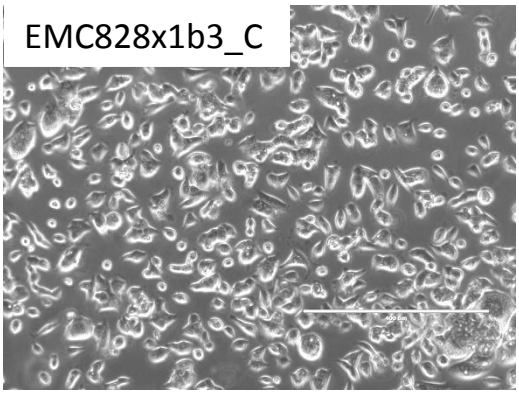

EMC828x2b2_C

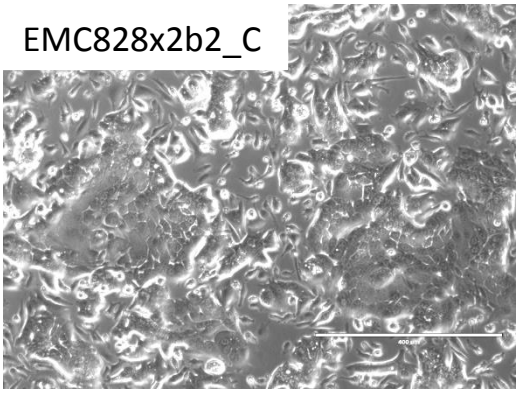

EMC828x2a3_C

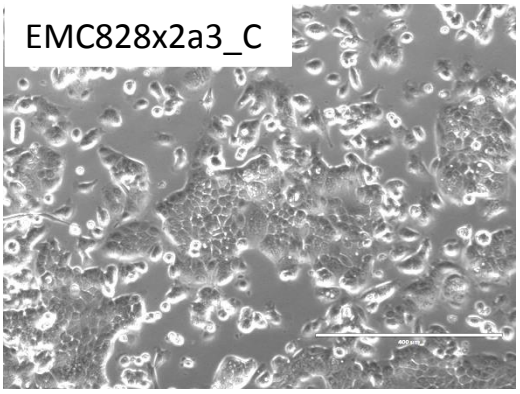

EMC41x2d2_C

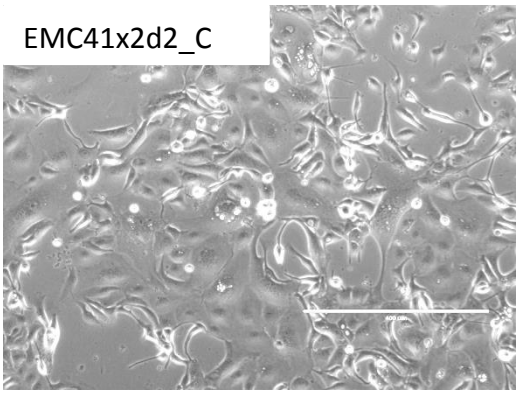

EMC41x1a3_C

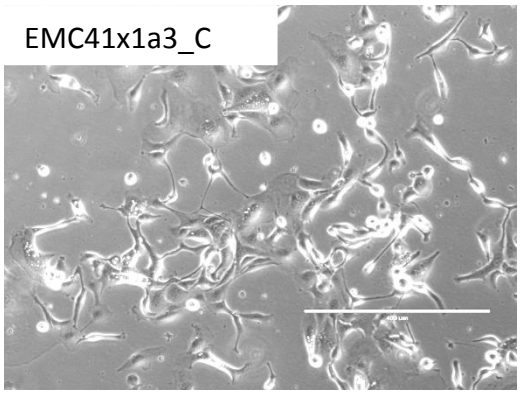

EMC41o3b3_C

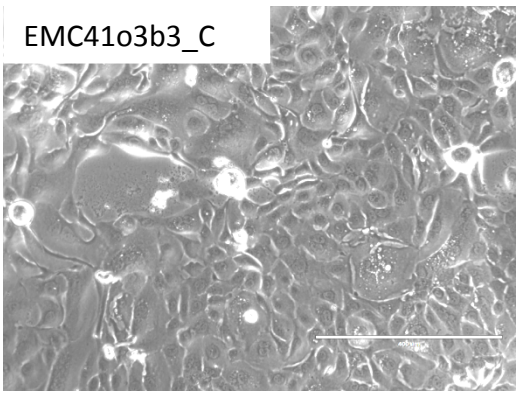

EMC29x1a1_C

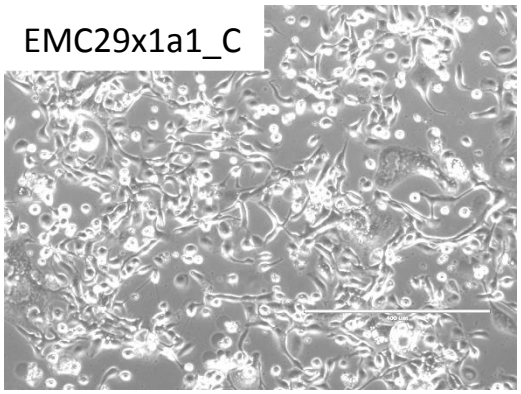

EMC29o1a2_C

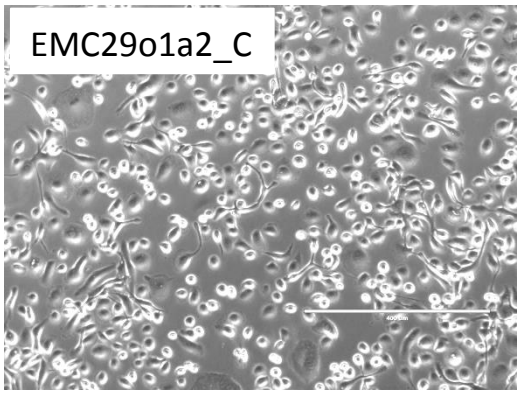

EMC29o1a1_C

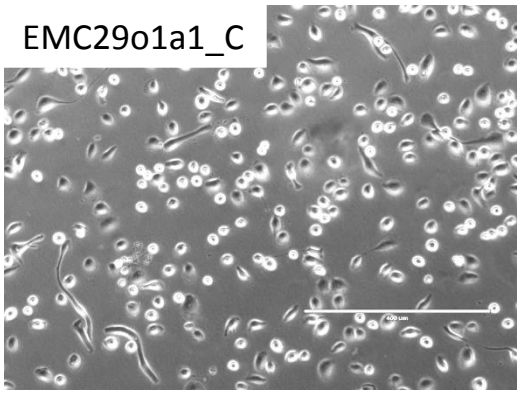

EMC29o1a5periMet_C

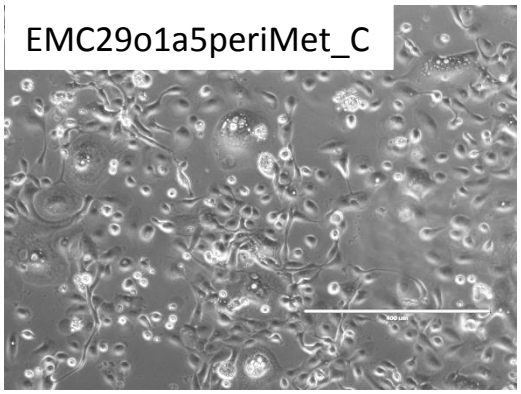

EMC114_C

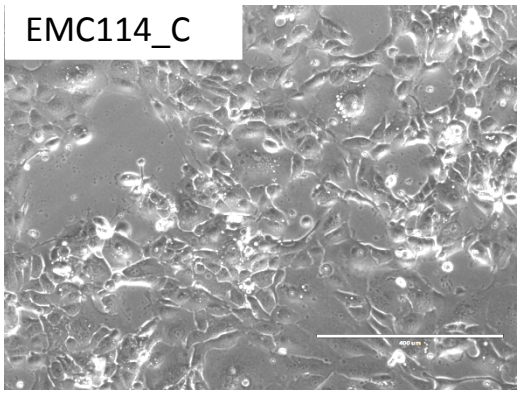

EMC114x1a1_C

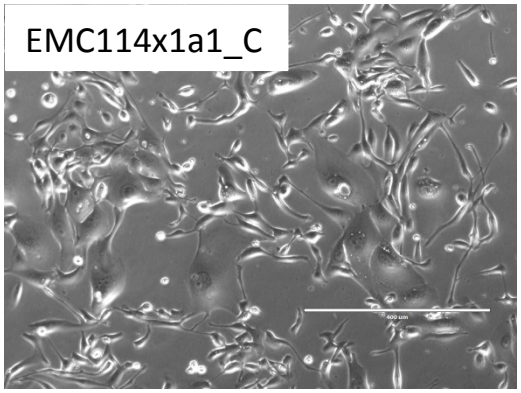

EMC114x2a4_C

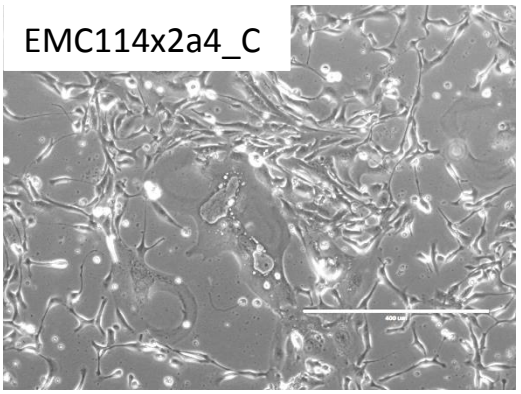

EMC114x2a3_C

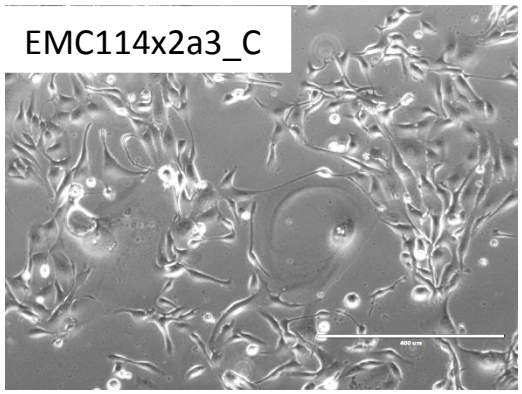

EMC519x1a2_C

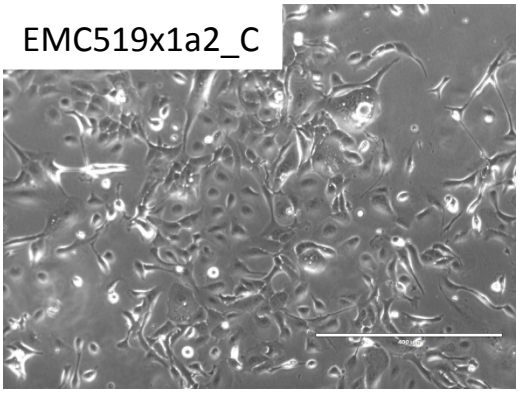

EMC519x1a3_C

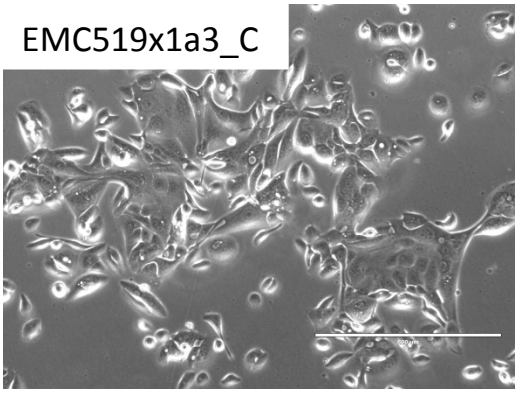

EMC519x2a1_C

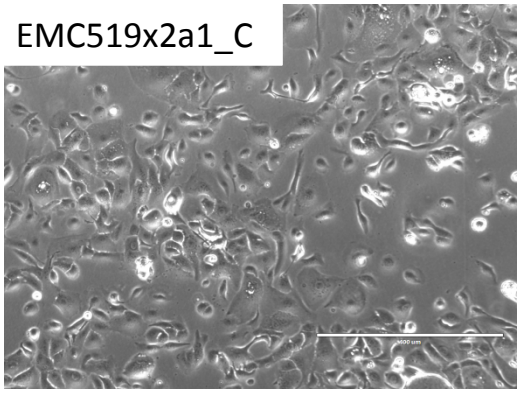

EMC810o1a1_C

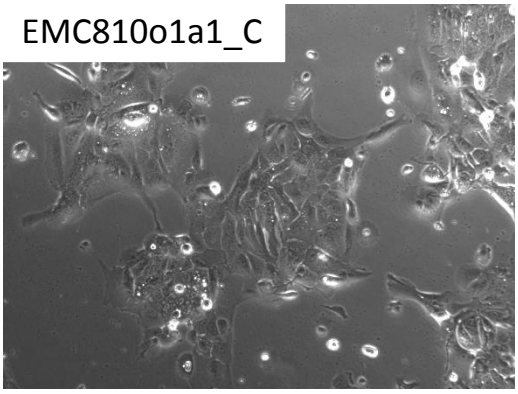

EMC33x4a2_C

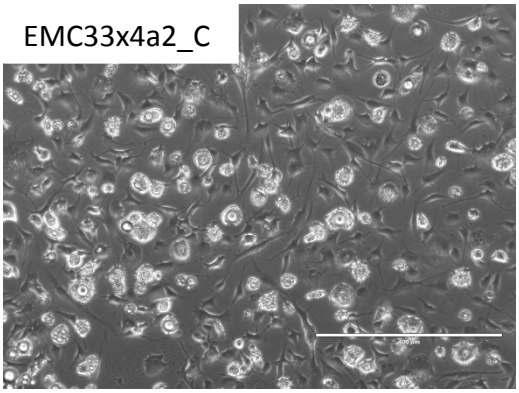

EMC35o1a5_C

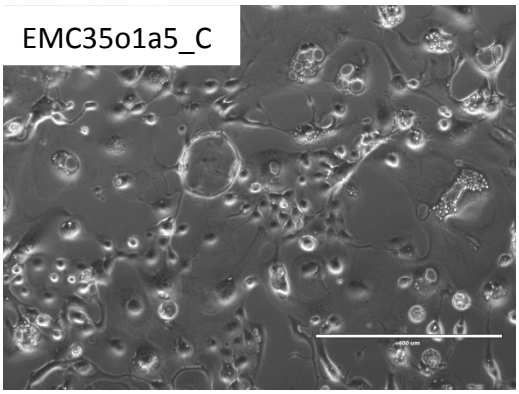

C.

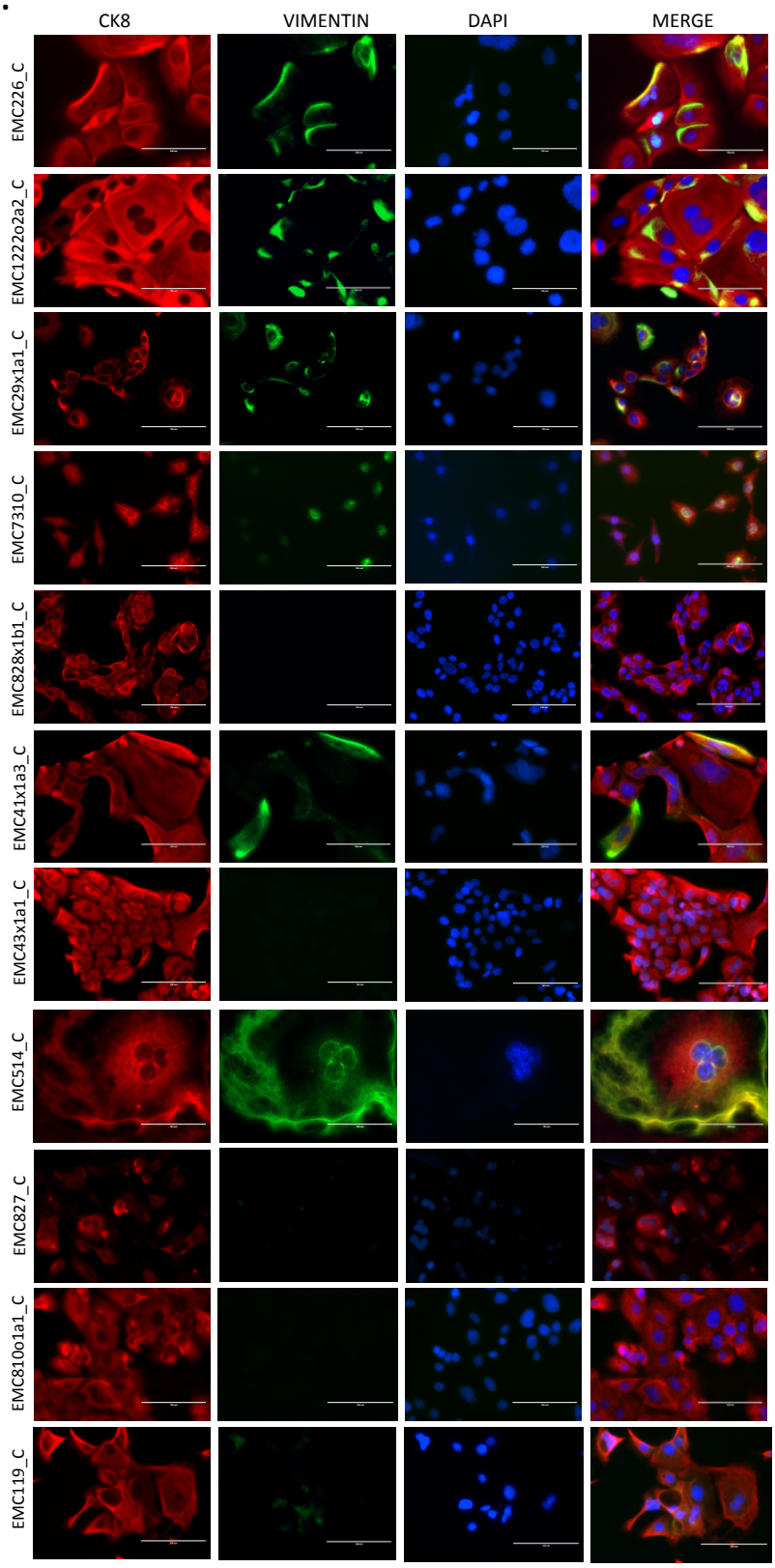

Cell line	%vimentin
EMC114_C	0
EMC519_C	1-5
EMCT2x1b1_C	0
EMC18128_C	80-90
EMC2095_C	30-40
EMC1229_C	80-90
EMC1229x1a2_C	15-20
EMC226_C	10-15
EMC1222o2a2_C	10-15
EMC29x1a1_C	15-20
EMC7310_C	10-15
EMC828x1b1_C	0
EMC41x1a3_C	20-25
EMC43x1a1_C	0
EMC514_C	50-60
EMC827_C	0-5
EMC810o1a1_C	0
EMC119_C	0-5

Late passage CK8

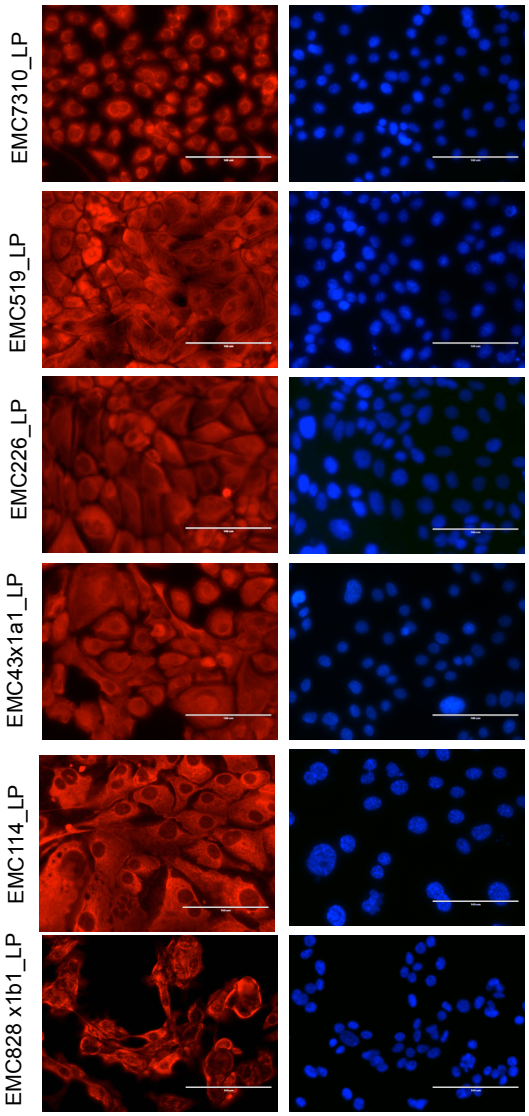

D.

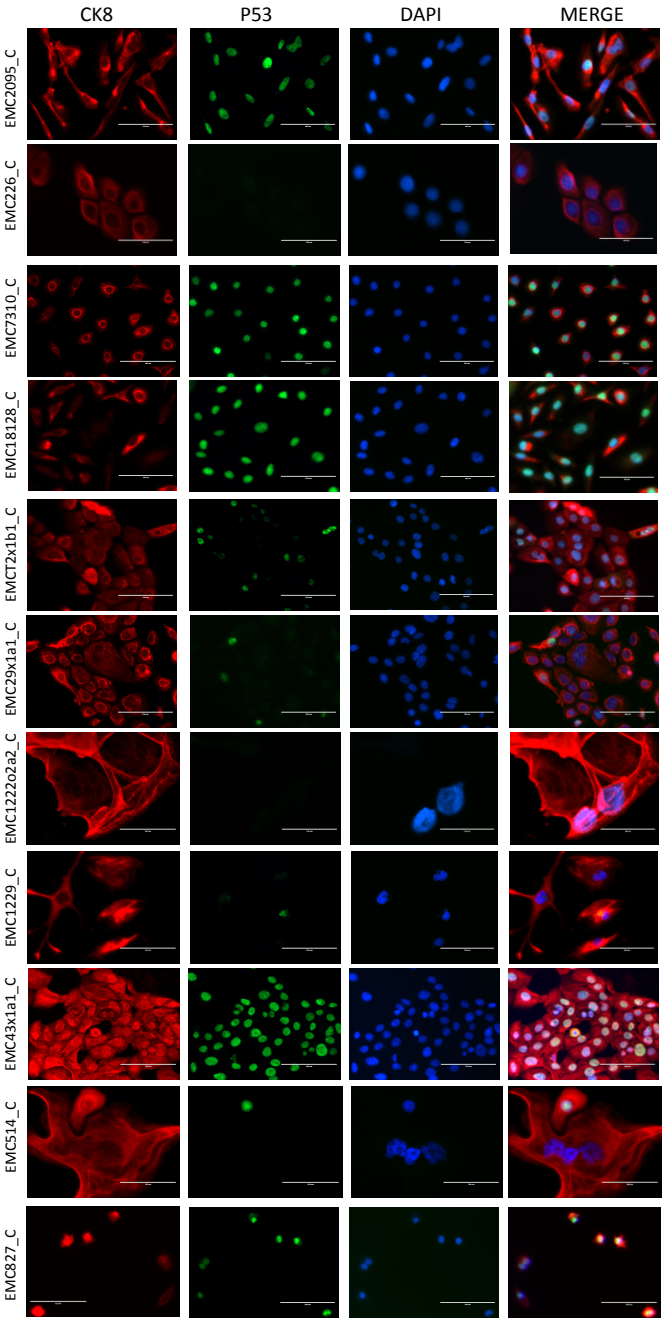

Cell line	%p53	TP53
EMC828x1b1_C	90-95	mut
EMC519_C	90-95	mut
EMC114_C	0	mut
EMC2095_C	80-90	indel
EMC226_C	1-5	indel
EMC7310_C	90-95	mut
EMC18128_C	80-90	mut
EMCT2x1b1_C	30-40	mut
EMC29x1a1_C	10-15	mut
EMC1222o2a2_C	5-10	wt
EMC1229_C	15-20	indel
EMC43x1a1_C	90-95	mut
EMC514_C	30-40	mut
EMC827_C	50-60	mut

E.

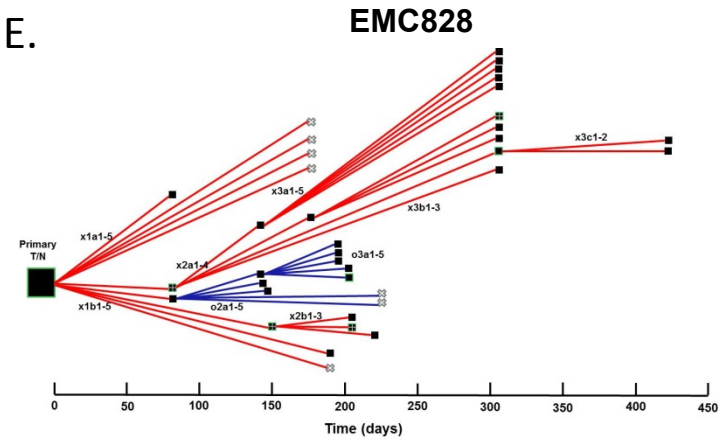
EMC828
Primary T/N
x1a1-5
x2a1-4
x3a1-5
x3b1-3
x3c1-2
o3a1-5
x1b1-5
o2a1-5
x2b1-3
0
50
100
150
200
250
300
350
400
450
Time (days)

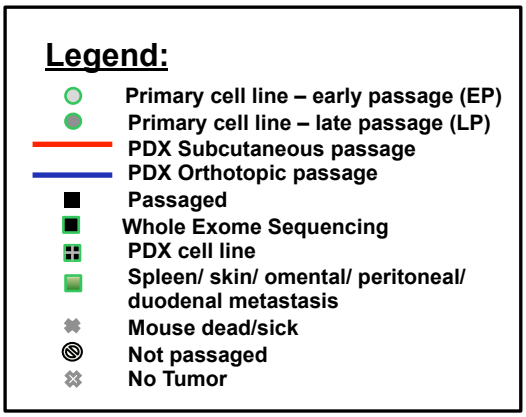
Legend:
Primary cell line – early passage (EP)
Primary cell line – late passage (LP)
PDX Subcutaneous passage
PDX Orthotopic passage
Passaged
Whole Exome Sequencing
PDX cell line
Spleen/ skin/ omental/ peritoneal/ duodenal metastasis
Mouse dead/sick
Not passaged
No Tumor

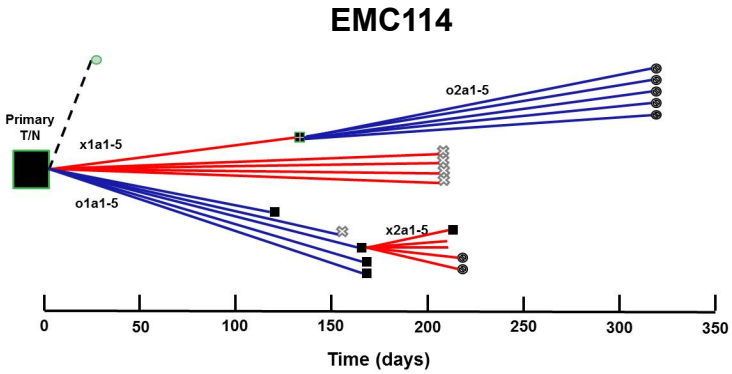
EMC114
Primary T/N
x1a1-5
o2a1-5
o1a1-5
x2a1-5
0
50
100
150
200
250
300
350
Time (days)

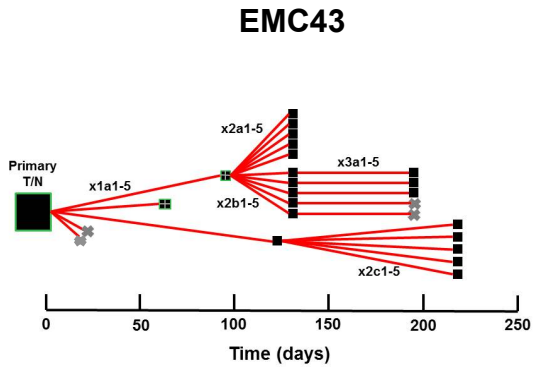
EMC43
Primary T/N
x1a1-5
x2a1-5
x3a1-5
x2b1-5
x2c1-5
0
50
100
150
200
250
Time (days)

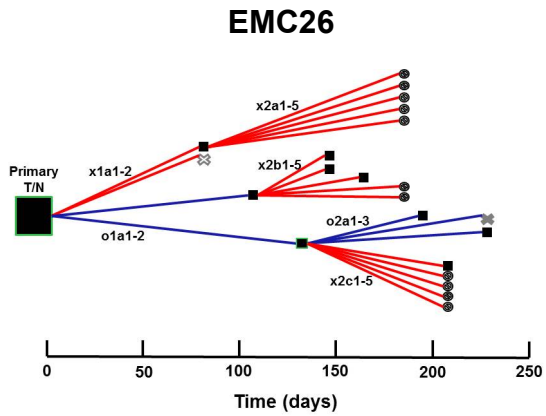
EMC26
Primary T/N
x1a1-2
x2a1-5
x2b1-5
o2a1-3
o1a1-2
x2c1-5
0
50
100
150
200
250
Time (days)

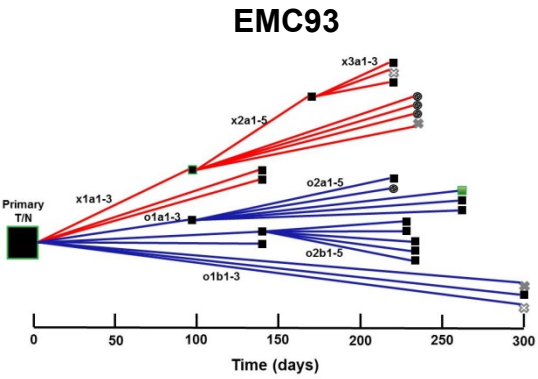
EMC93
Primary T/N
x3a1-3
x2a1-5
x1a1-3
o1a1-3
o2a1-5
o2b1-5
o1b1-3
0
50
100
150
200
250
300
Time (days)

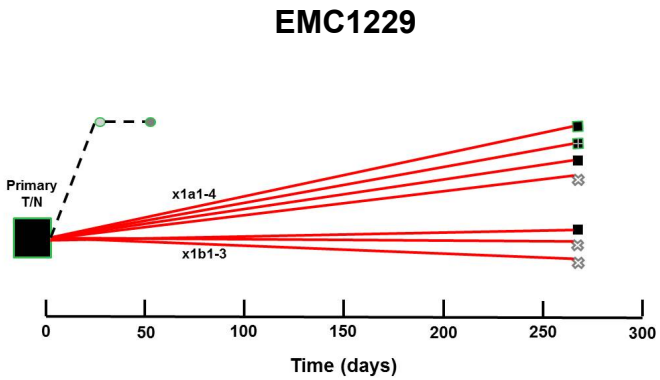
EMC1229
Primary T/N
x1a1-4
x1b1-3
0
50
100
150
200
250
300
Time (days)

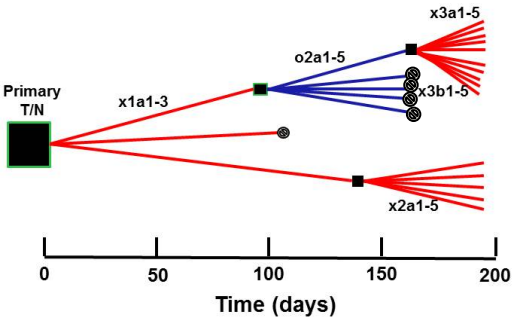
EMC62
Primary T/N
x1a1-3
o2a1-5
x3a1-5
x3b1-5
x2a1-5
0
50
100
150
200
Time (days)

EMC41

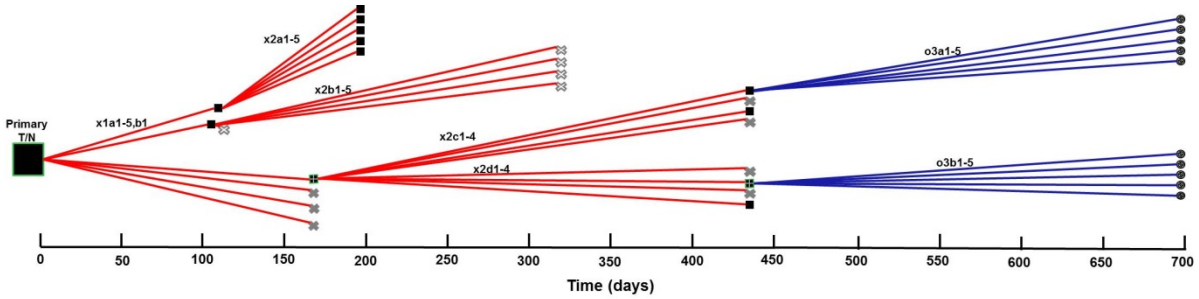

EMC519

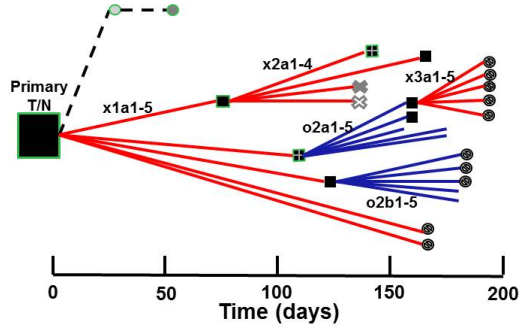

EMC129

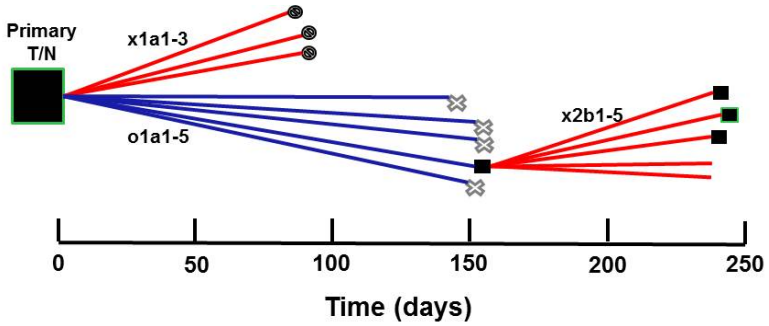

EMC810

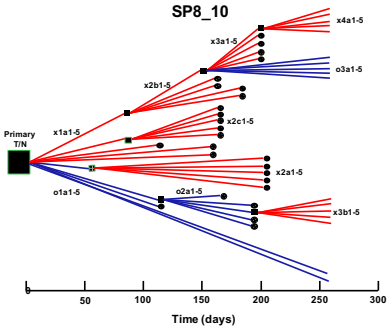

EMC29

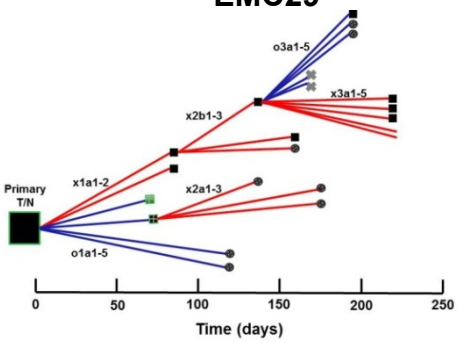

EMC827

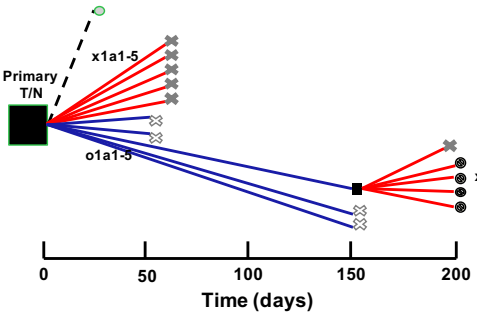

EMC33

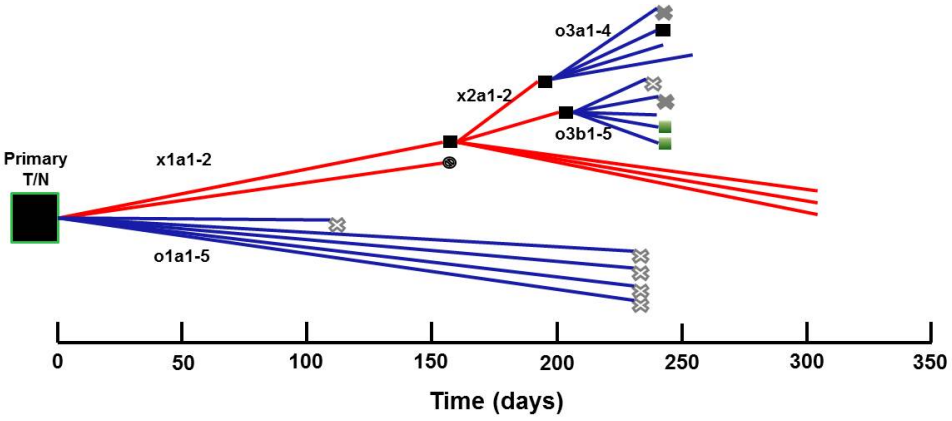

EMC1022

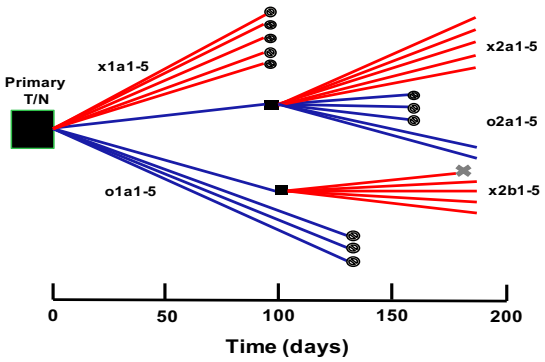

EMC1012

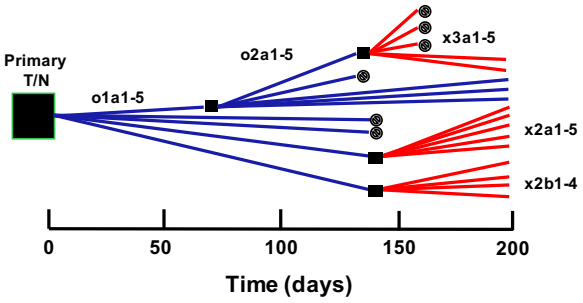

EMC319

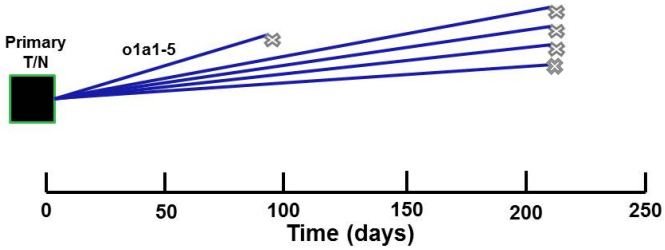

EMC528

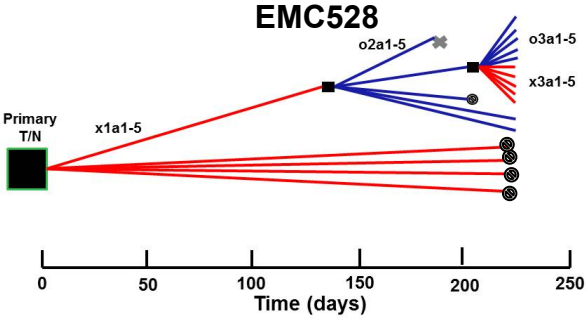

EMC119

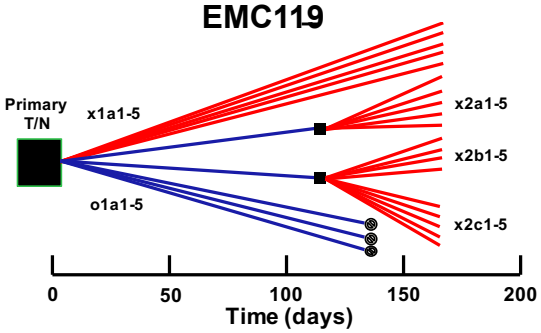

EMC35

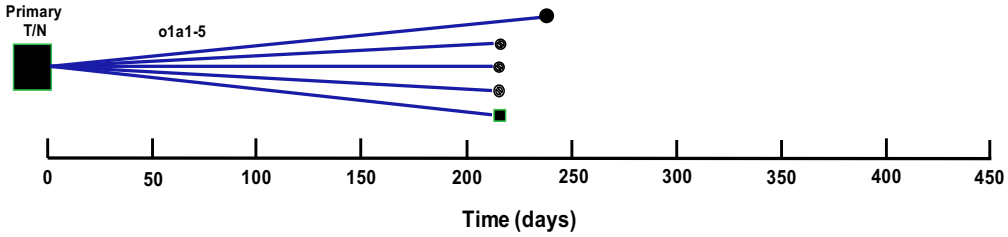

F.

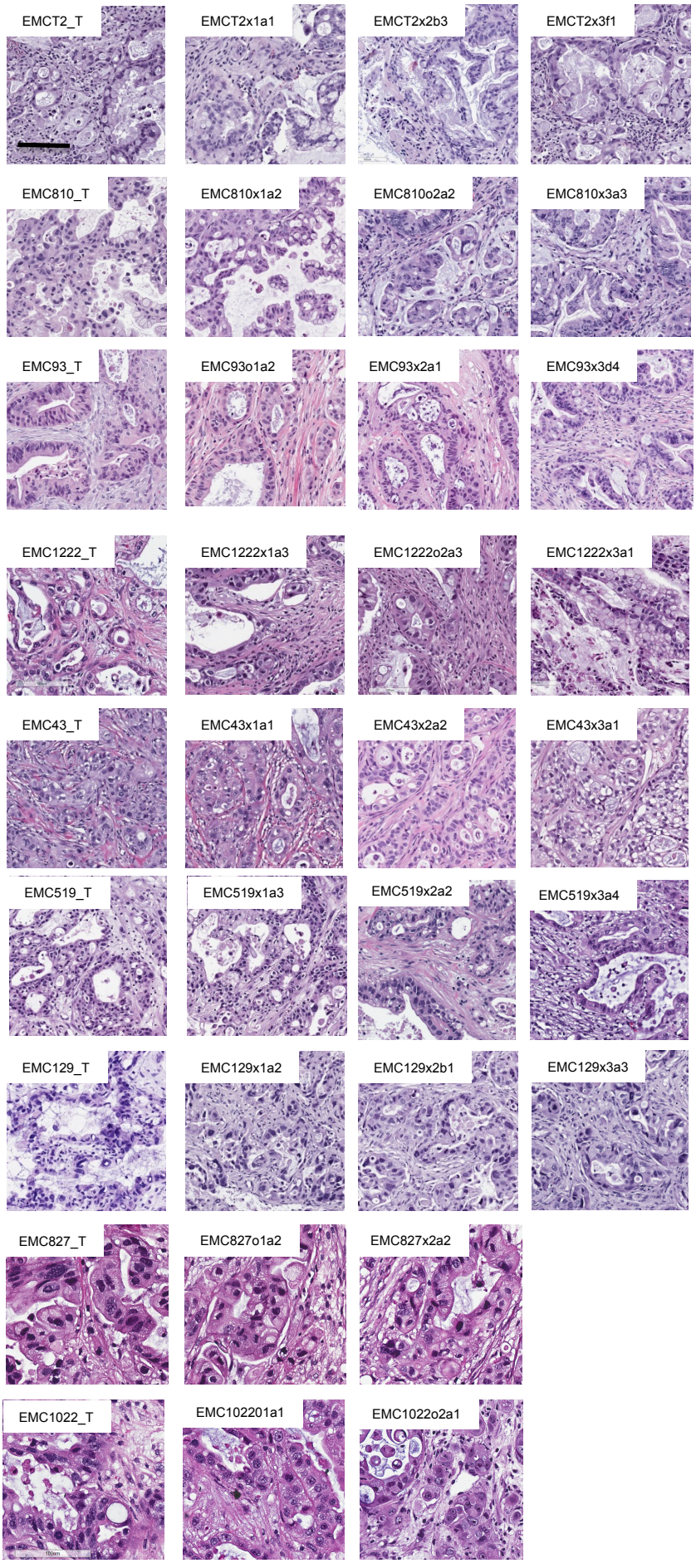
EMCT2_T
EMCT2x1a1
EMCT2x2b3
EMCT2x3f1
EMC810_T
EMC810x1a2
EMC810o2a2
EMC810x3a3
EMC93_T
EMC93o1a2
EMC93x2a1
EMC93x3d4
EMC1222_T
EMC1222x1a3
EMC1222o2a3
EMC1222x3a1
EMC43_T
EMC43x1a1
EMC43x2a2
EMC43x3a1
EMC519_T
EMC519x1a3
EMC519x2a2
EMC519x3a4
EMC129_T
EMC129x1a2
EMC129x2b1
EMC129x3a3
EMC827_T
EMC827o1a2
EMC827x2a2
EMC1022_T
EMC102201a1
EMC1022o2a1

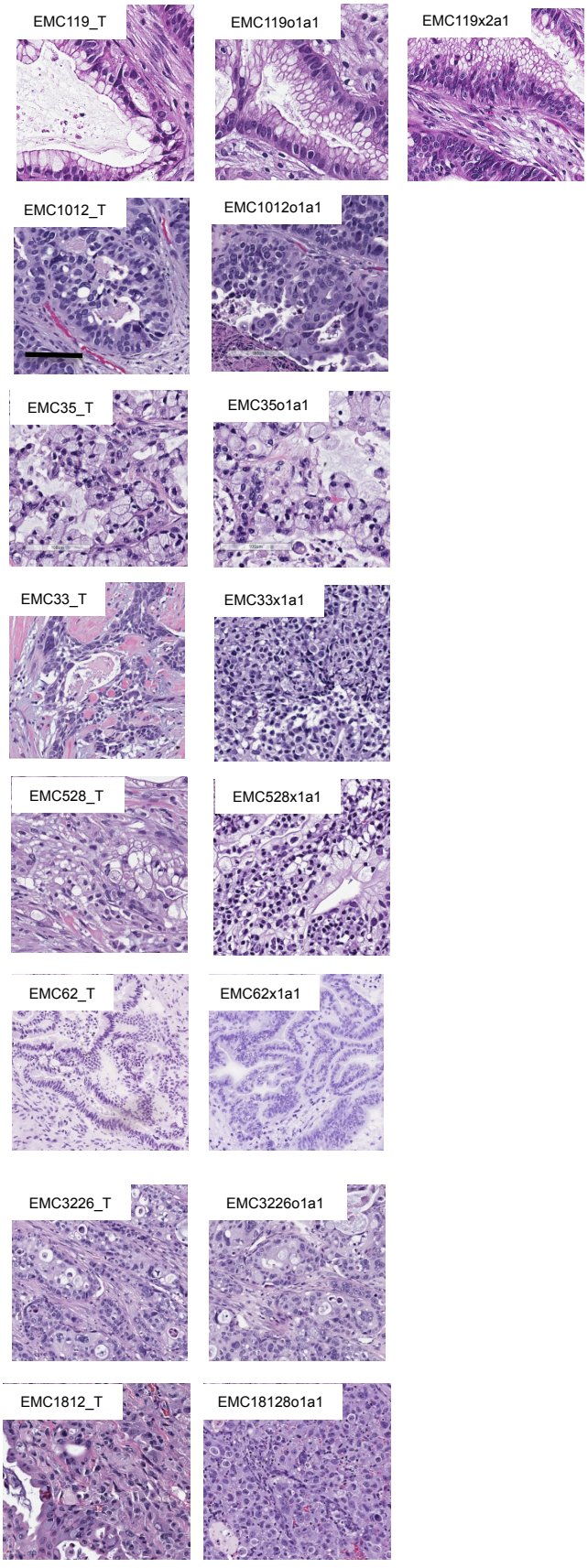
EMC119_T
EMC119o1a1
EMC119x2a1
EMC1012_T
EMC1012o1a1
EMC35_T
EMC35o1a1
EMC33_T
EMC33x1a1
EMC528_T
EMC528x1a1
EMC62_T
EMC62x1a1
EMC3226_T
EMC3226o1a1
EMC1812_T
EMC18128o1a1

A.

Cell Line	Collison et al.
EMC810_T	CLASSIC
EMC1229_T	QASI MESENCHYMAL
EMC514_T	EXOCRINE
EMC41_T	CLASSIC
EMC828_T	CLASSIC
EMC18128_T	QASI MESENCHYMAL
EMC2095_T	QASI MESENCHYMAL
EMC7310_T	QASI MESENCHYMAL
EMC43_T	CLASSIC
EMC519_T	CLASSIC
EMC827_T	QASI MESENCHYMAL
EMC1222_T	CLASSIC
EMC29_T	CLASSIC
EMC114_T	CLASSIC
EMC226_T	QASI MESENCHYMAL
EMC3226_T	EXOCRINE
EMCT2_T	QASI MESENCHYMAL

B.

Alterations between passages & Comparison to primary T

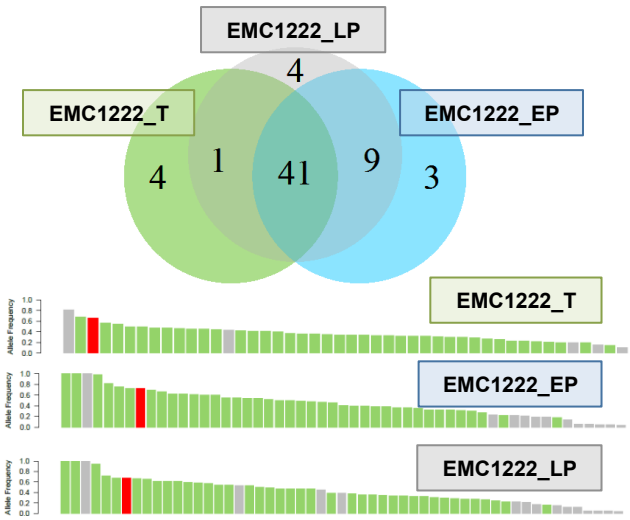

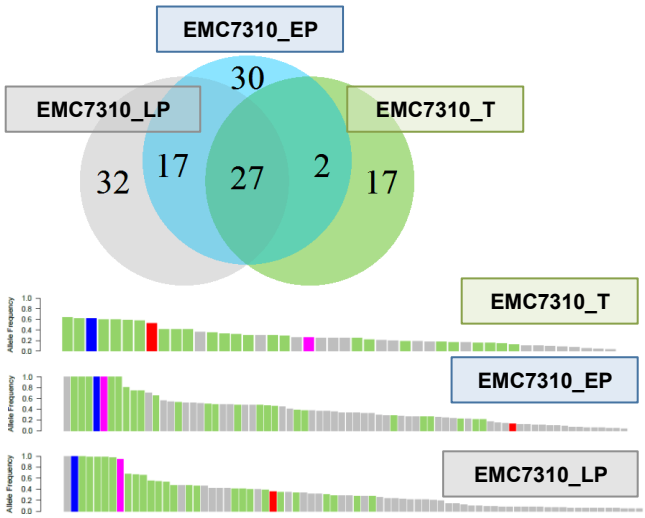

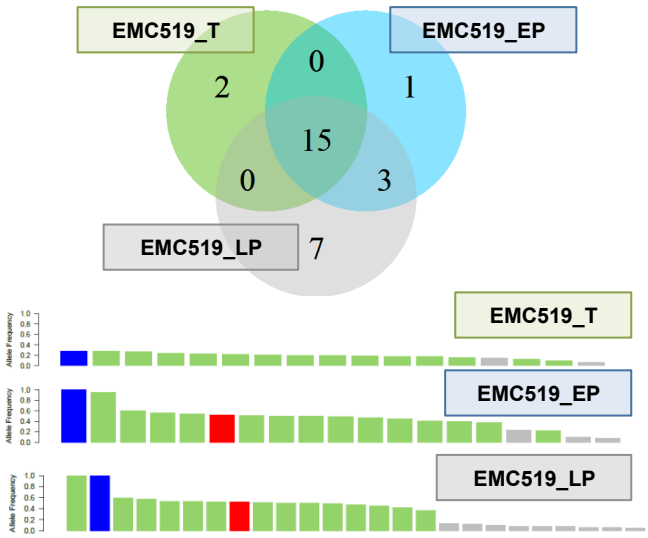

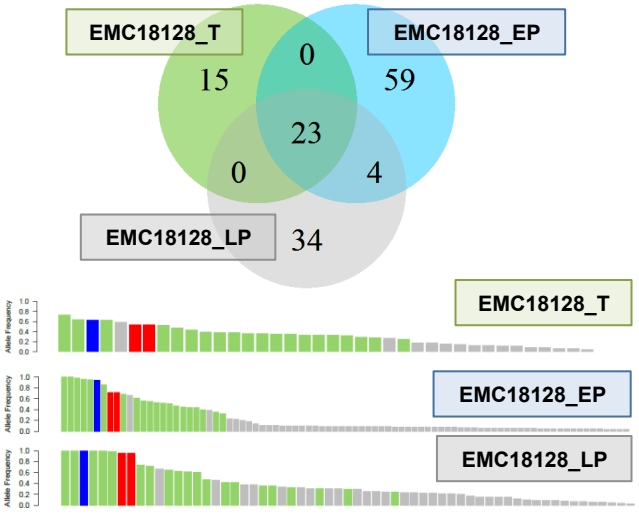

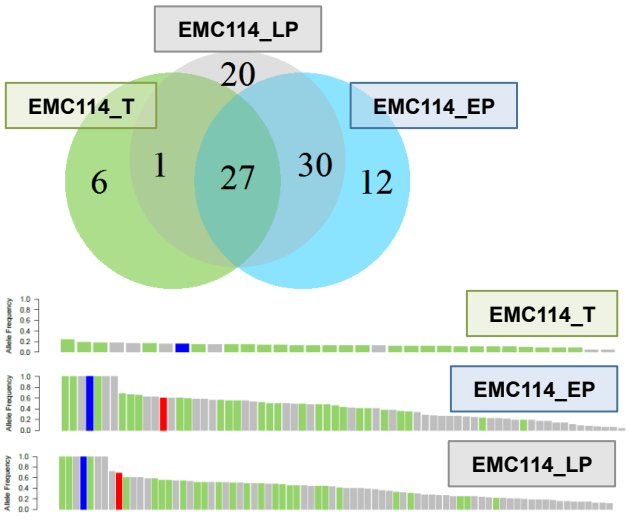

The case has two mutations in KRAS effecting codon 12**

C.

Analysis of tumor variants present in tumor and LP, but not EP

EMC1222_EP

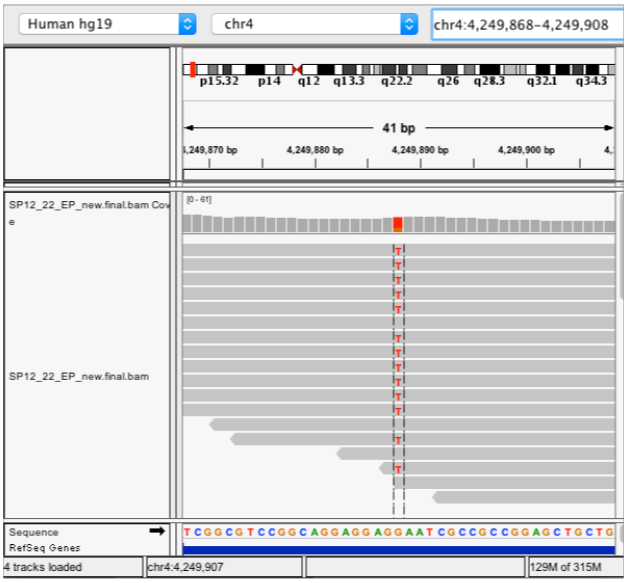

In model EMC1222 a SNV in the TMEM128 gene is not called in the early passage cell line due strand bias.

EMC114_EP

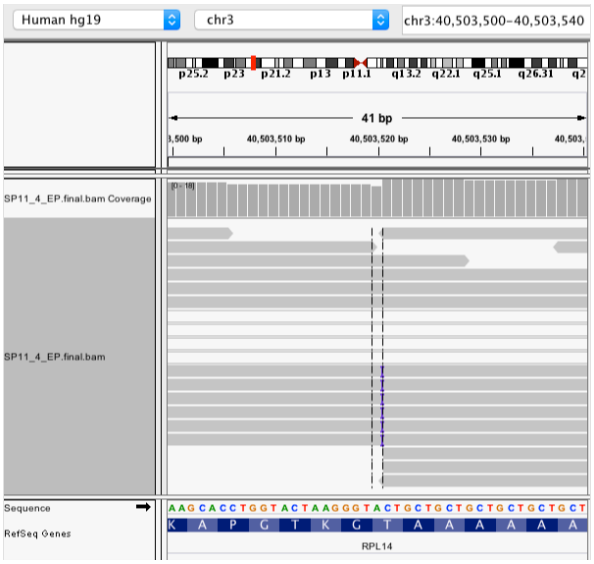

In model EMC114 an indel in the RPL14 gene is not called in the early passage cell line due to low coverage at this site.

D.

Correlation heatmap between primary T and primary Cell lines

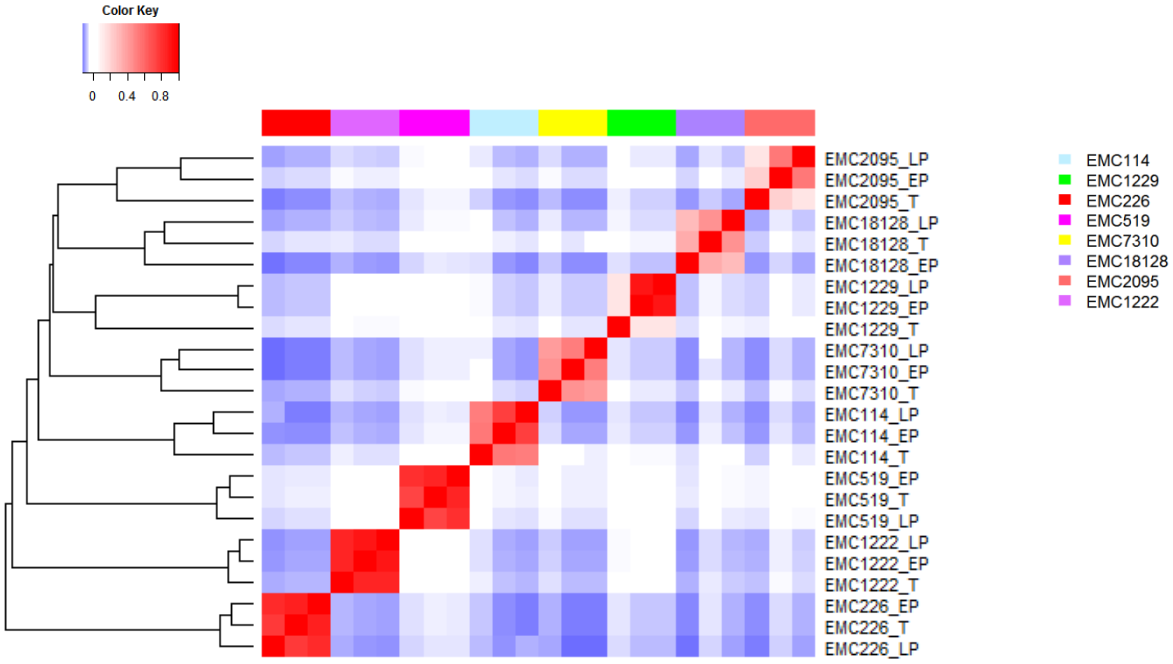

Alterations between mice (same passage different mice)

E.

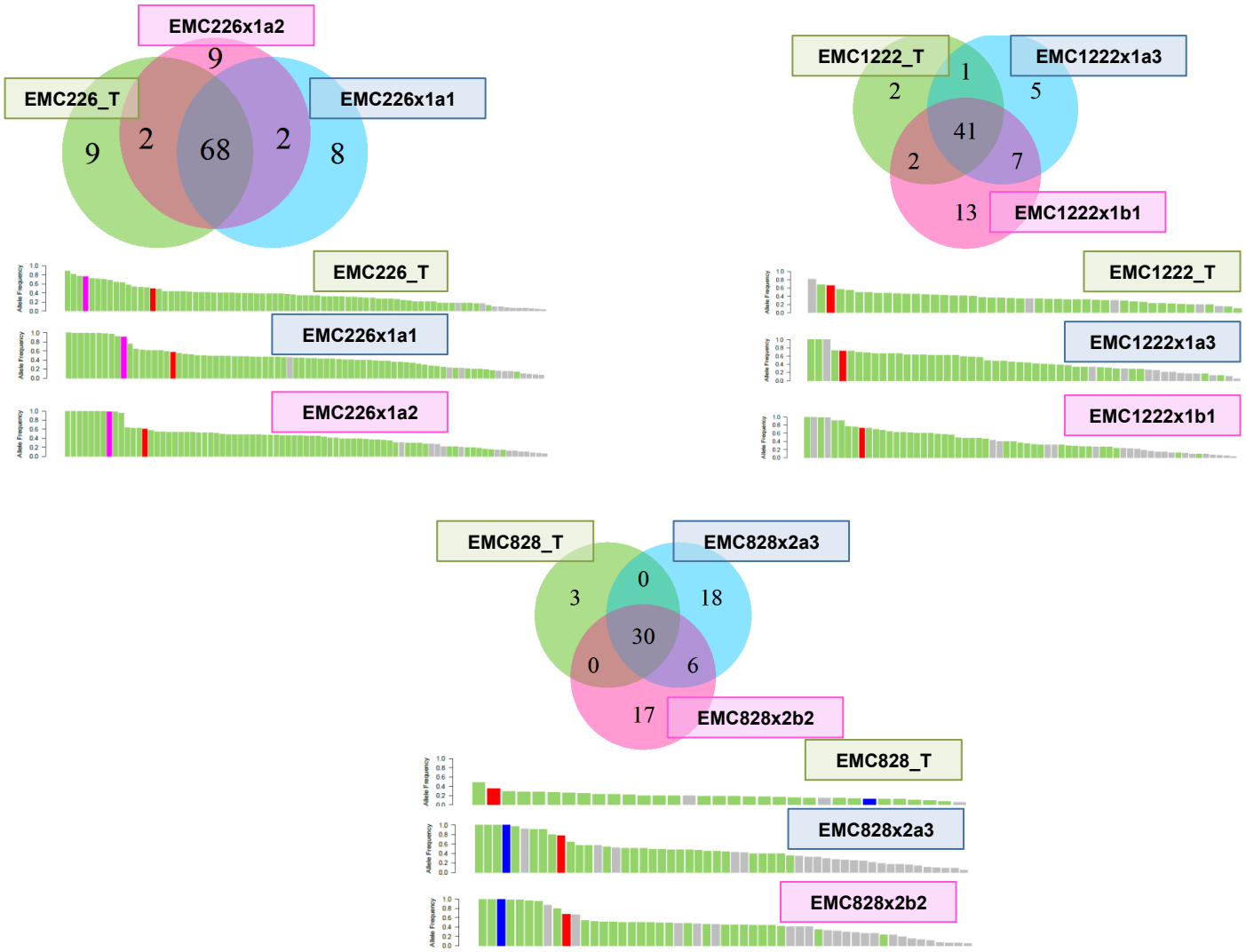

Correlation heatmap between primary T and PDX

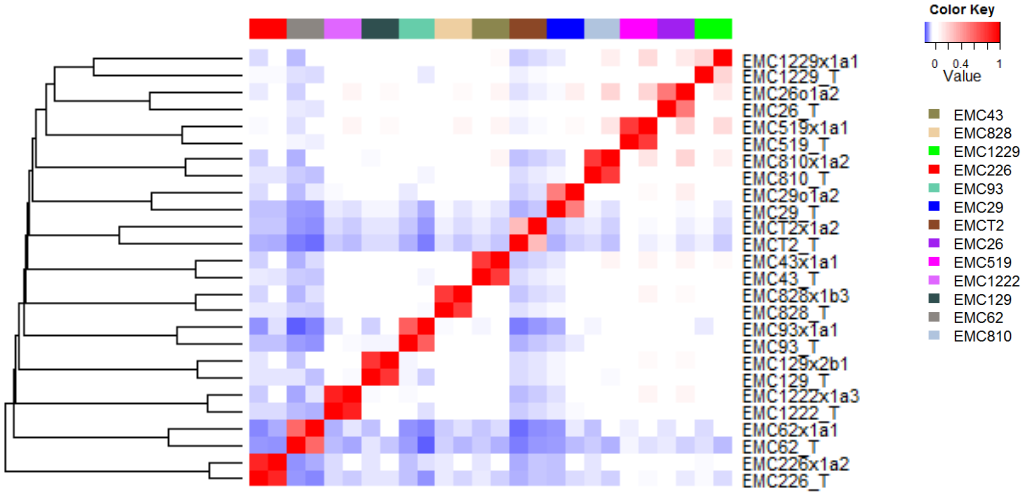

Alterations with passage and metastasis

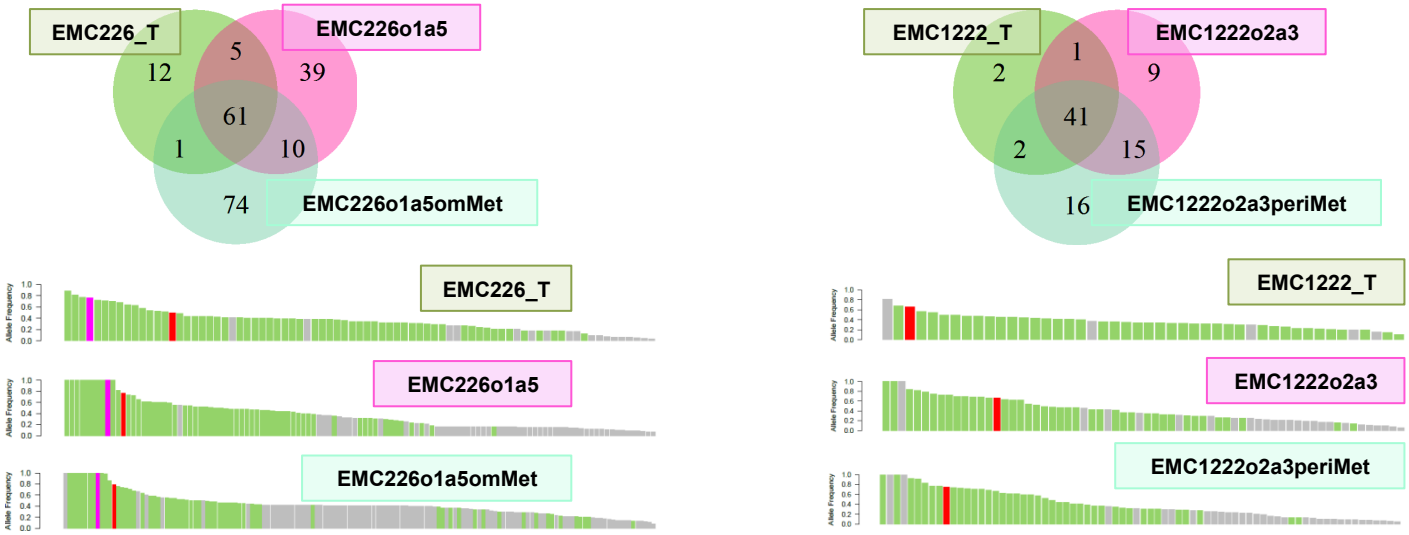

Correlation heatmap between primary T and metastasis

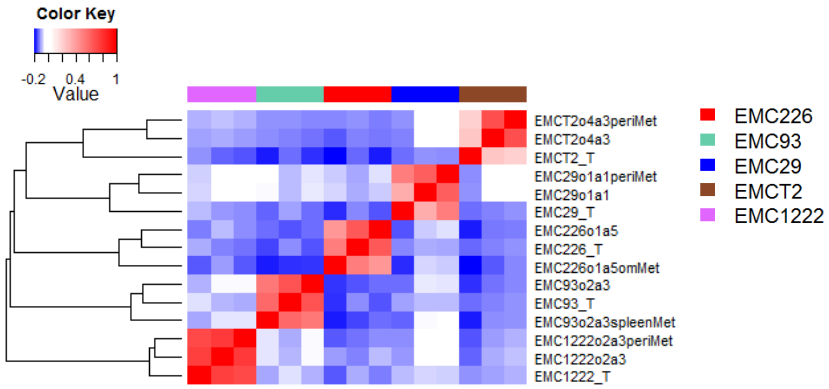

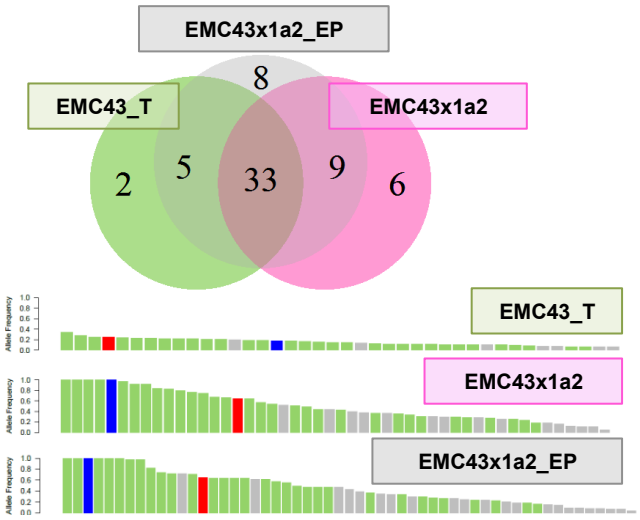

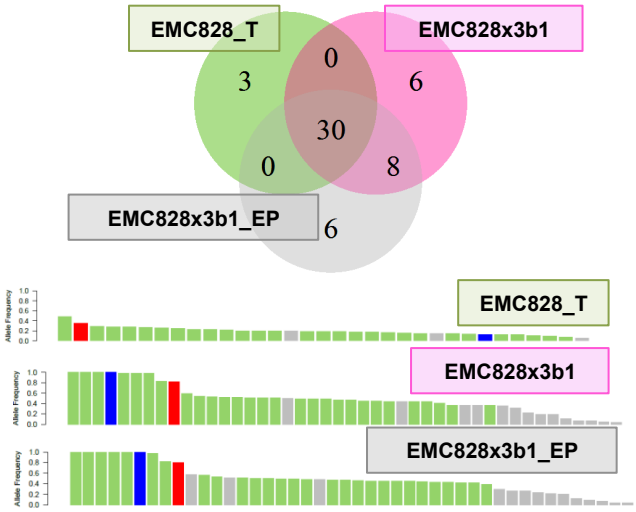

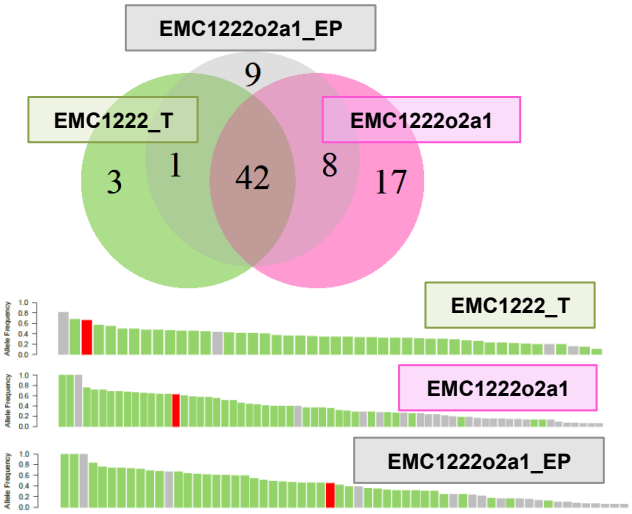

Correlation heatmap between primary T , PDX and PDX derived Cell lines

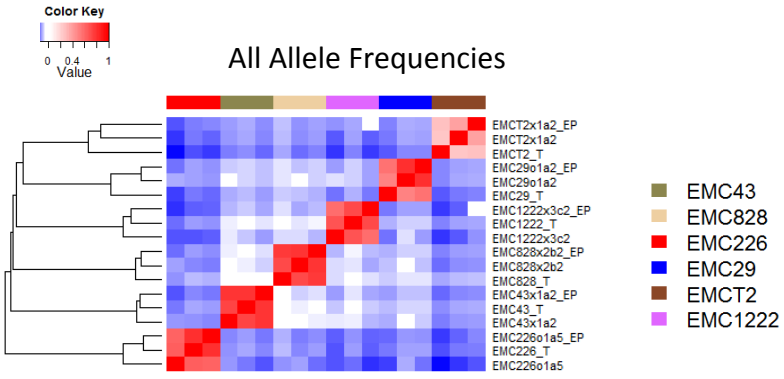

PDX derived Cell lines

Alterations between passages & Comparison to primary T

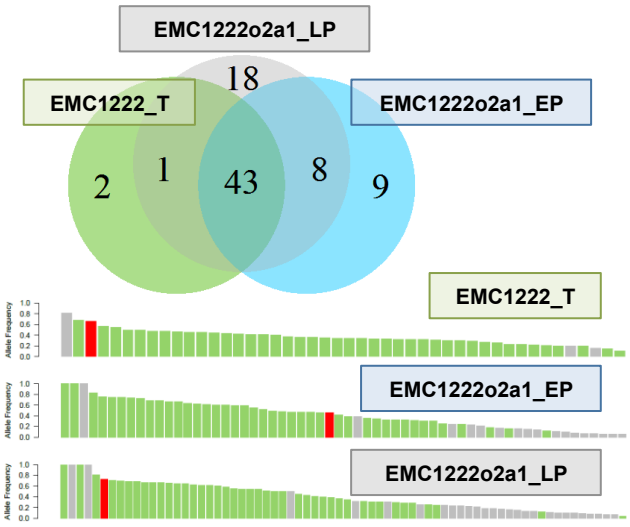

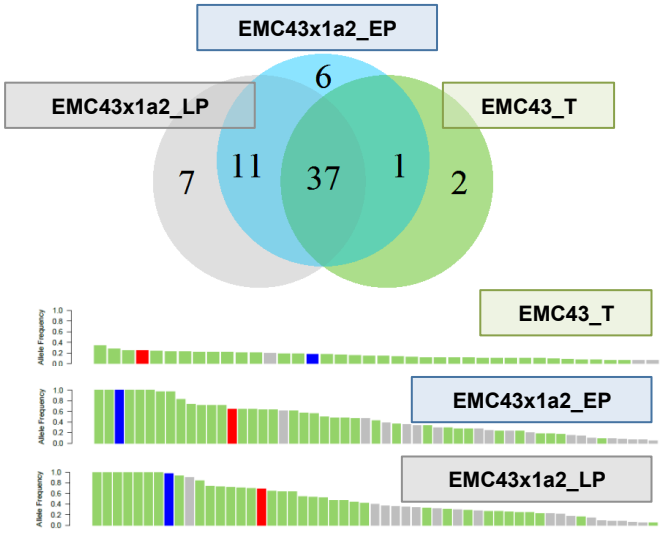

Correlation heatmap between primary T and PDX derived Cell lines

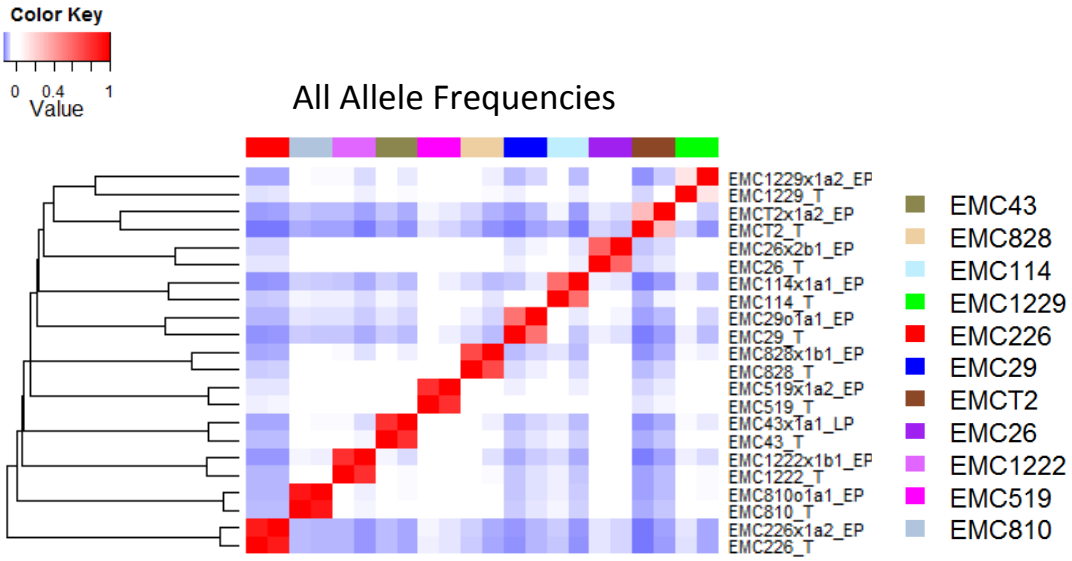

F.

Heterogeneity of EMC12_29 histology

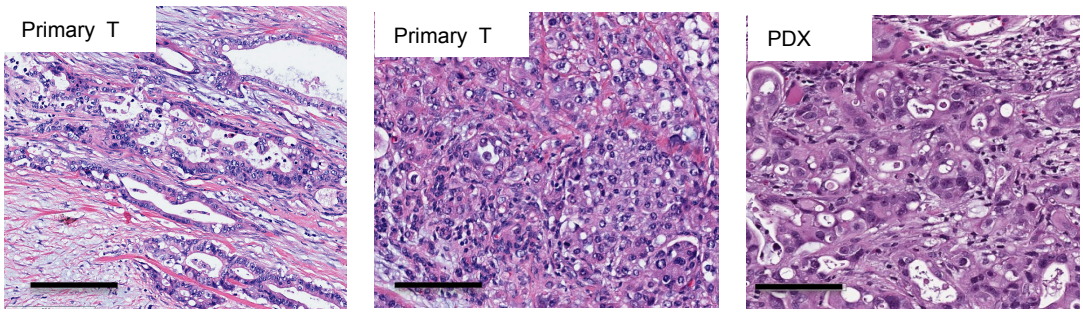

A.

Tumor Case	Model SNV Summary (C=common, UX=unique to xenograft, UT=unique to tumor)	C	UX	UT
EMC26_T	o1a2	14	18	8
EMC35_T	o1a5	14	13	2
EMC62_T	x1a1	81	49	38
EMC129_T	x1b1	29	7	7
EMC519_T	x1a1	16	9	2
EMC810_T	x1a2	33	17	7
EMC18128	o1a1	23	29	15
EMC43_T	x1a1	32	16	8
EMC43_T	x1a2	33	15	7
EMT2_T	x1a2	30	41	45
EMT2_T	x2b1	31	40	2
EMT2_T	o4a3	30	50	2
EMT2_T	o4a3 peritMet	25	45	2
EMC93_T	x1a1	54	50	7
EMC93_T	o2a3	54	41	7
EMC93_T	o2a3 periMet	50	26	11
EMC93_T	o2a3 spleenMet	51	53	10
EMC226_T	x1a1	68	10	11
EMC226_T	x1a2	70	11	9
EMC226_T	o1a5	66	49	13
EMC226_T	o1a5met	62	84	17
EMC29_T	o1a2	28	14	35
EMC29_T	o1a1 liverMet	25	11	38
EMC29_T	o1a1 peritMet	30	17	33
EMC29_T	o1a1 liverMet_1	30	52	33
EMC29_T	o1a1 spleenMet	30	39	33
EMC828_T	x1b1	29	26	4
EMC828_T	x1b3	30	16	3
EMC828_T	x2a3	30	24	3
EMC828_T	x2b2	30	23	3
EMC828_T	x3b1	30	14	3
EMC828_T	o3a5	28	19	5
EMC1222_T	x1a3	42	12	4
EMC1222_T	x1b1	43	20	3
EMC1222_T	x3a1	42	44	4
EMC1222_T	x3c2	42	39	4
EMC1222_T	o2a1	42	25	4
EMC1222_T	o2a2	42	26	4
EMC1222_T	o2a3	42	24	4
EMC1222_T	o2a3 omentalMet	42	28	4
EMC1222_T	o2a3 spleenMet	42	39	4
EMC1222_T	o2a3 skinMet	43	42	3
EMC1222_T	o2a3 duodenalMet	41	39	5
EMC1222_T	o2a3 peritonealMet	43	31	3

B.

PDX

Mutant Allele Frequency Scatterplots

EMC226

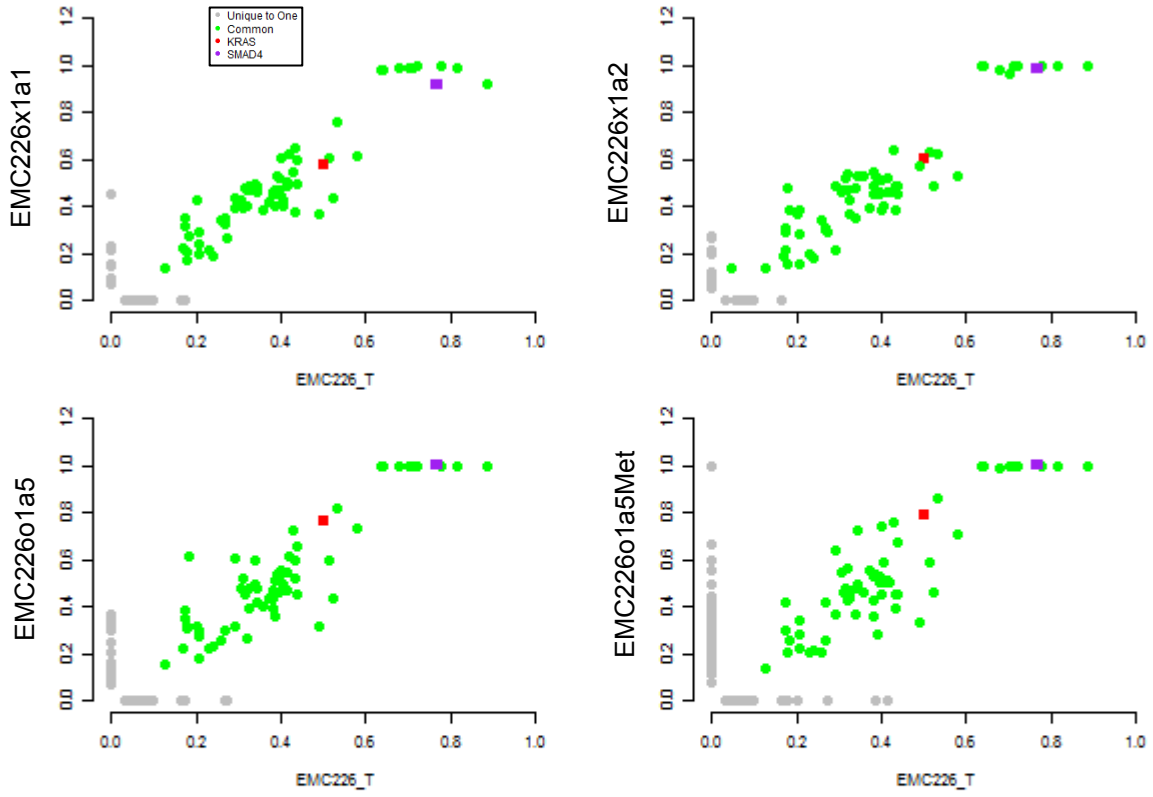

EMC1222

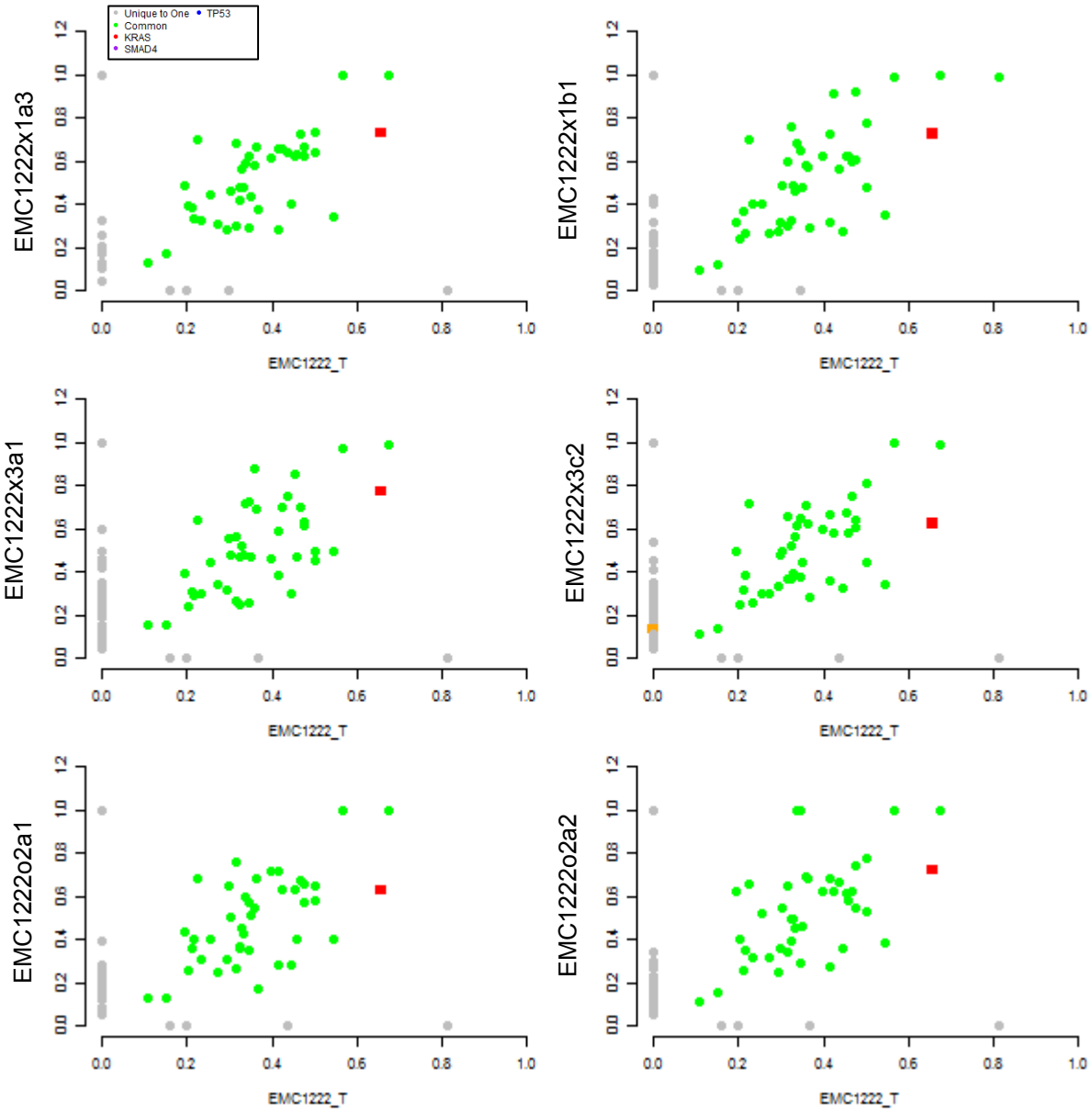
Unique to One
TP53
Common
KRAS
SMAD4
EMC1222x1a3
EMC1222x1b1
EMC1222x3a1
EMC1222x3c2
EMC1222o2a1
EMC1222o2a2
EMC1222_T
0.0
0.2
0.4
0.6
0.8
1.0
1.2

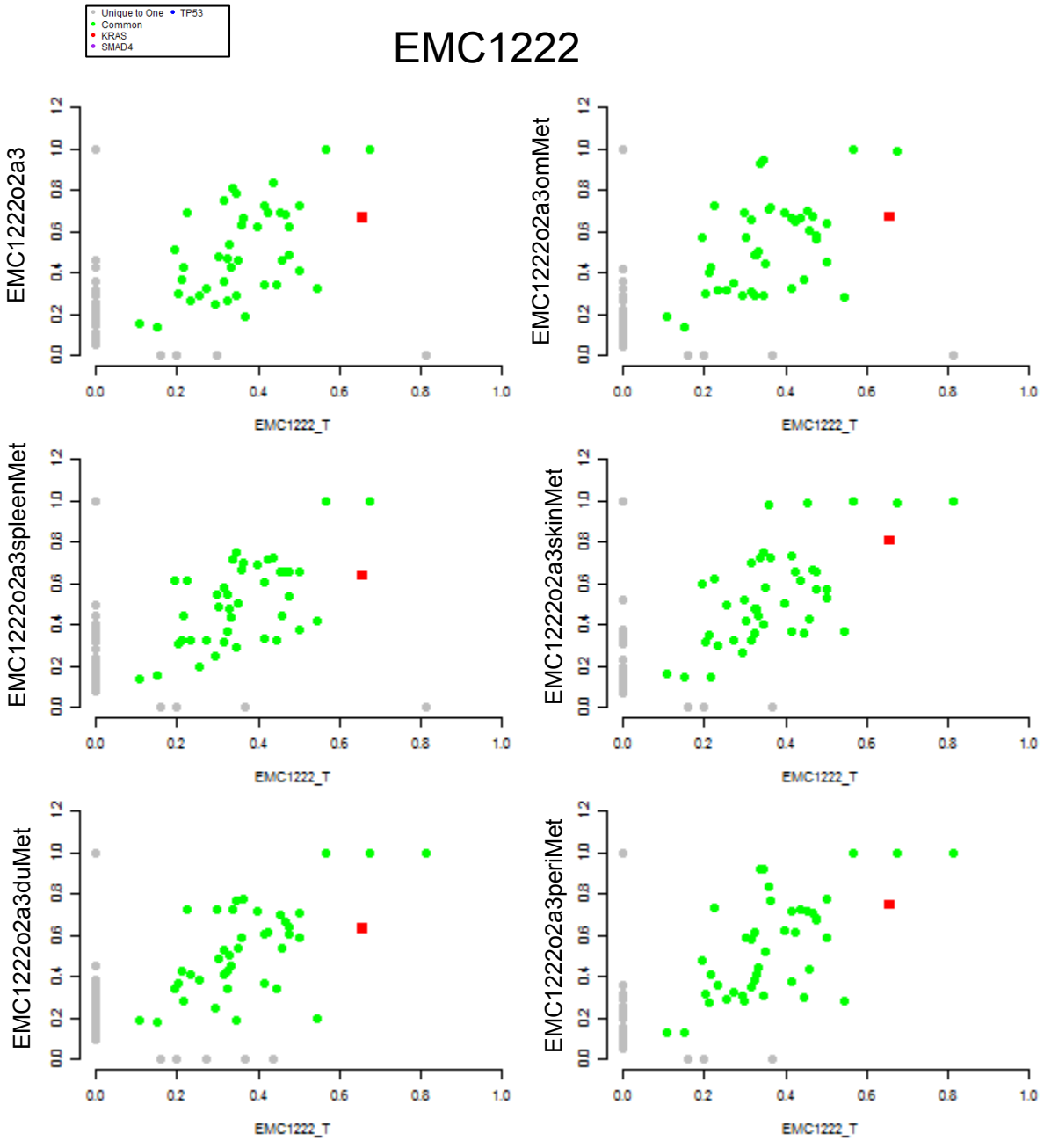
EMC1222
Unique to One
TP53
Common
KRAS
SMAD4
EMC1222o2a3
EMC1222o2a3omMet
EMC1222o2a3spleenMet
EMC1222o2a3skinMet
EMC1222o2a3duMet
EMC1222o2a3periMet
EMC1222_T

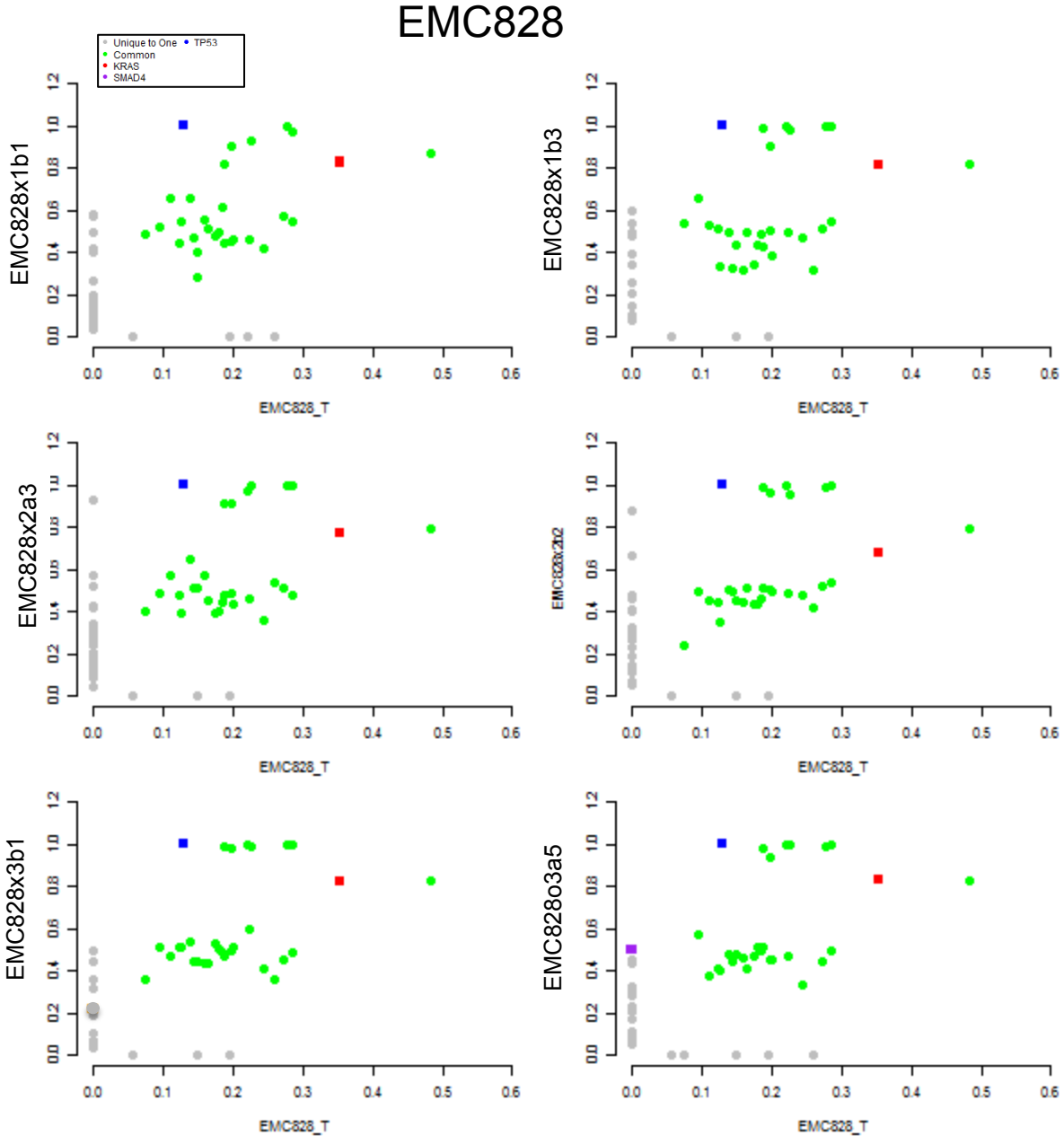
EMC828
Unique to One
TP53
Common
KRAS
SMAD4
EMC828x1b1
EMC828x1b3
EMC828x2a3
EMC828x3b1
EMC828o3a5
EMC828_T

EMC29

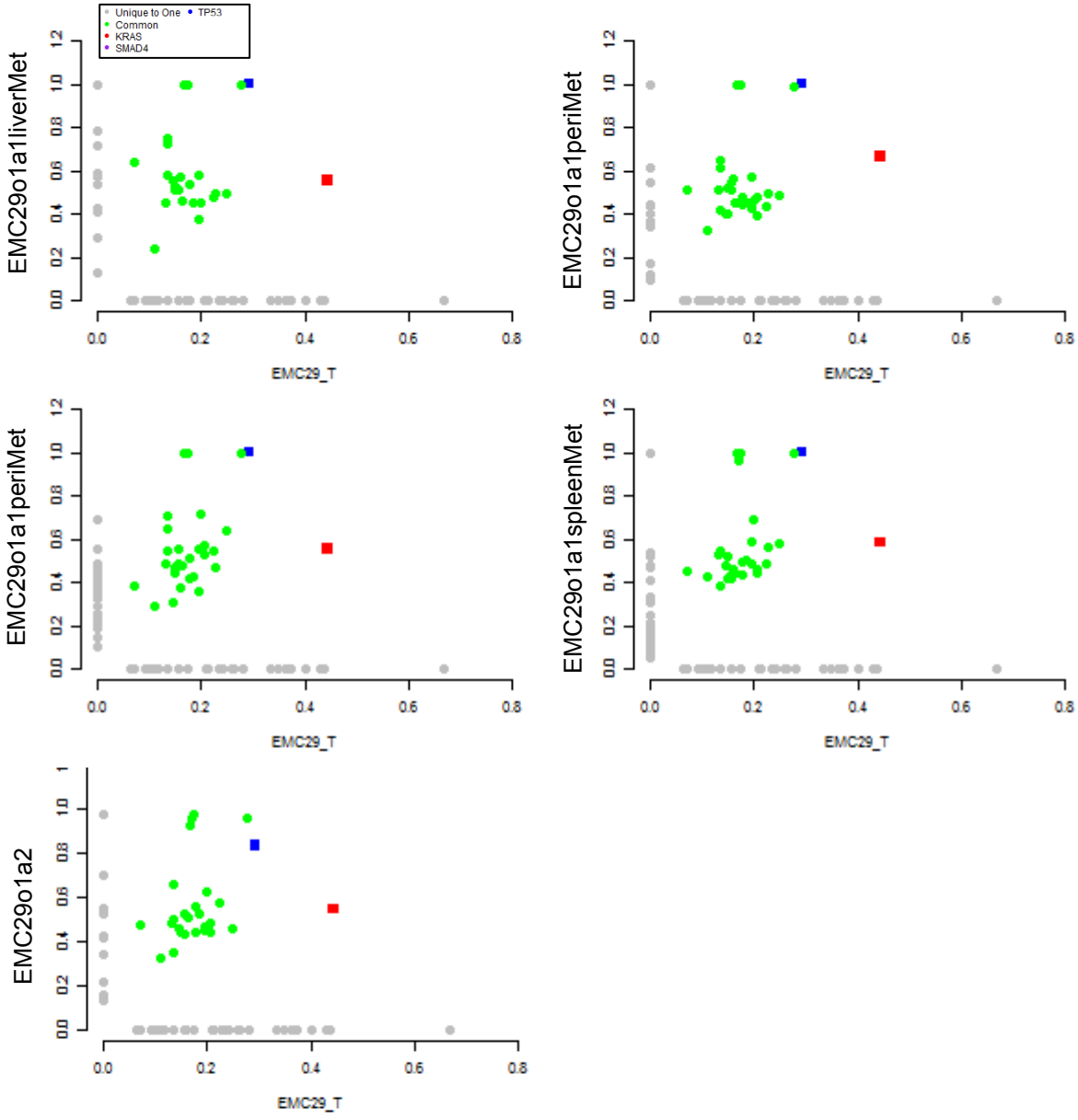
Unique to One
TP53
Common
KRAS
SMAD4
EMC29o1a1liverMet
EMC29o1a1periMet
EMC29o1a1periMet
EMC29o1a1spleenMet
EMC29o1a2
EMC29_T

EMC26

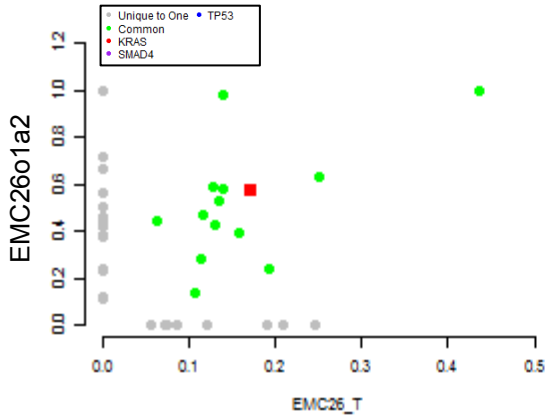

EMC35

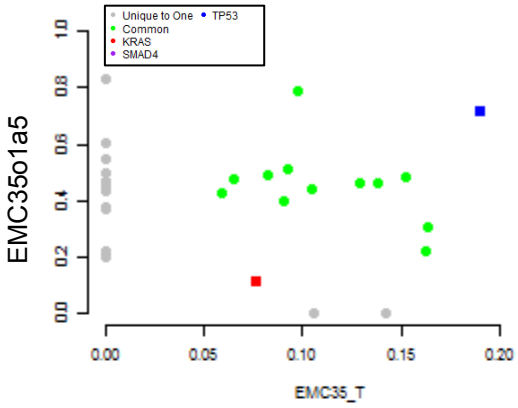

EMC43

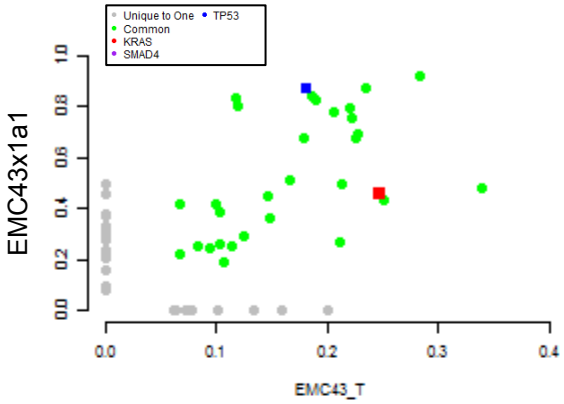

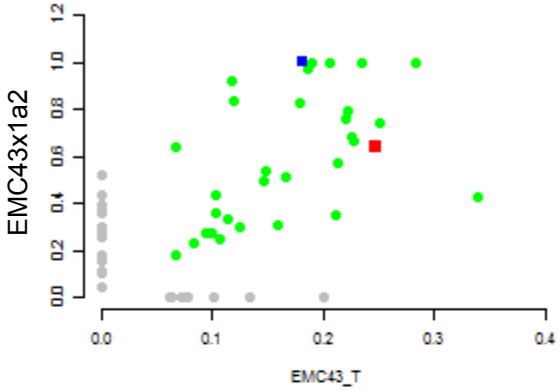

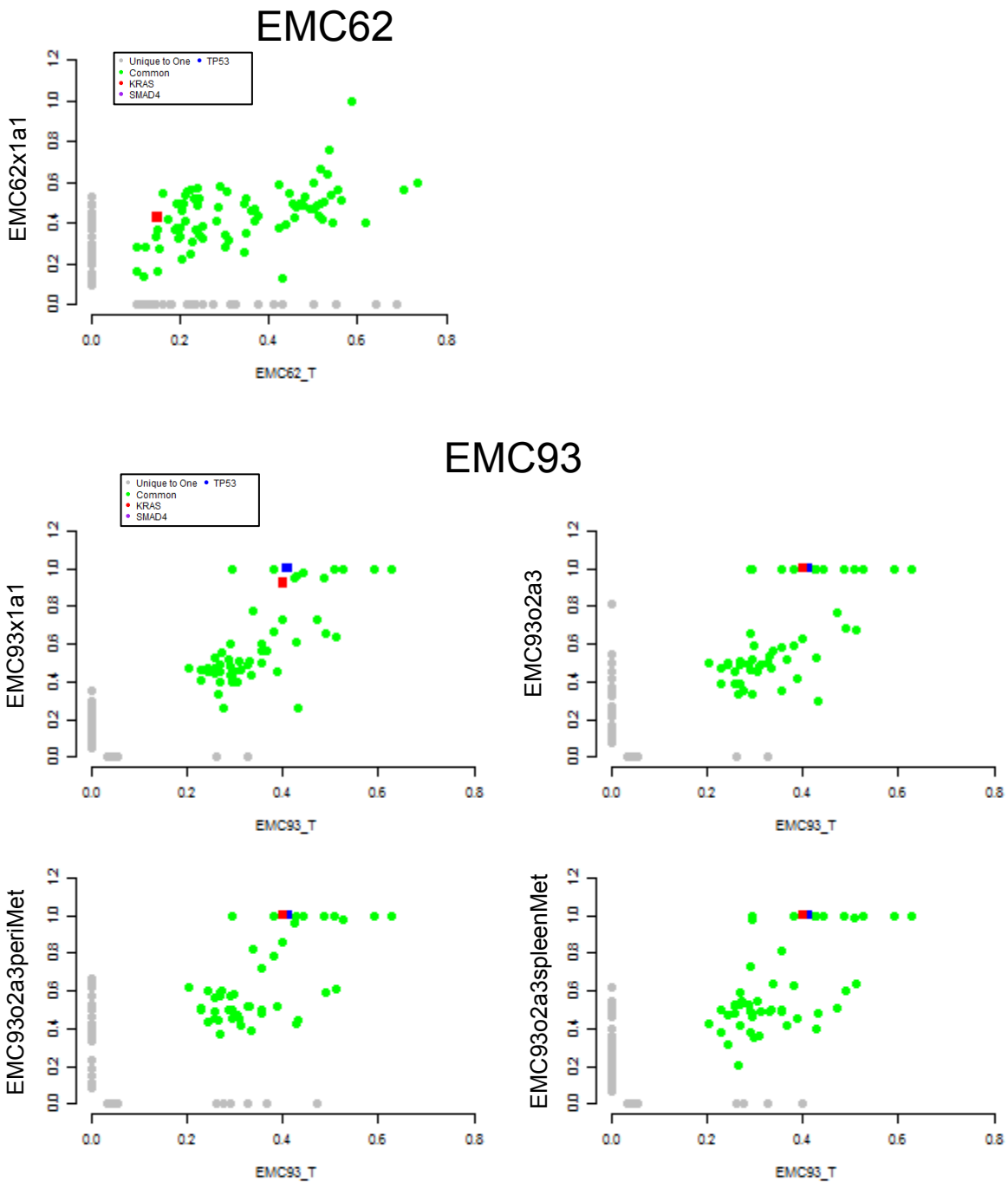
EMC62
Unique to One
TP53
Common
KRAS
SMAD4
EMC62x1a1
EMC62_T
EMC93
EMC93x1a1
EMC93o2a3
EMC93o2a3periMet
EMC93o2a3spleenMet
EMC93_T

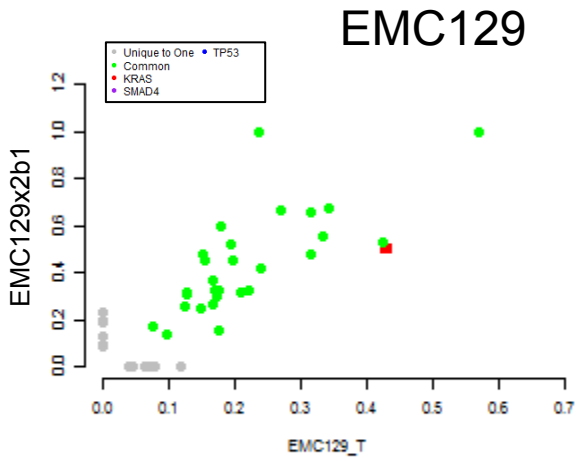
EMC129
Unique to One
TP53
Common
KRAS
SMAD4
EMC129x2b1
EMC129_T
0.0
0.2
0.4
0.6
0.8
1.0
1.2
0.1
0.3
0.5
0.7

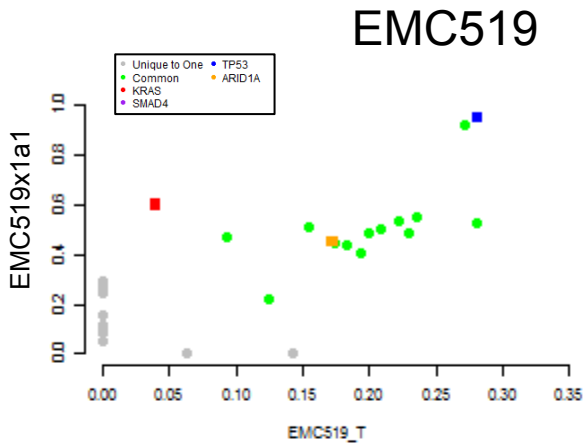
EMC519
Unique to One
TP53
Common
ARID1A
KRAS
SMAD4
EMC519x1a1
EMC519_T
0.00
0.05
0.10
0.15
0.20
0.25
0.30
0.35

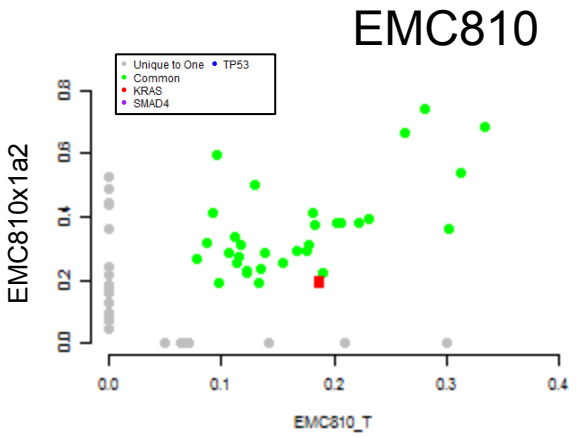
EMC810
Unique to One
TP53
Common
KRAS
SMAD4
EMC810x1a2
EMC810_T
0.0
0.2
0.4
0.6
0.8
0.1
0.3

EMCT2

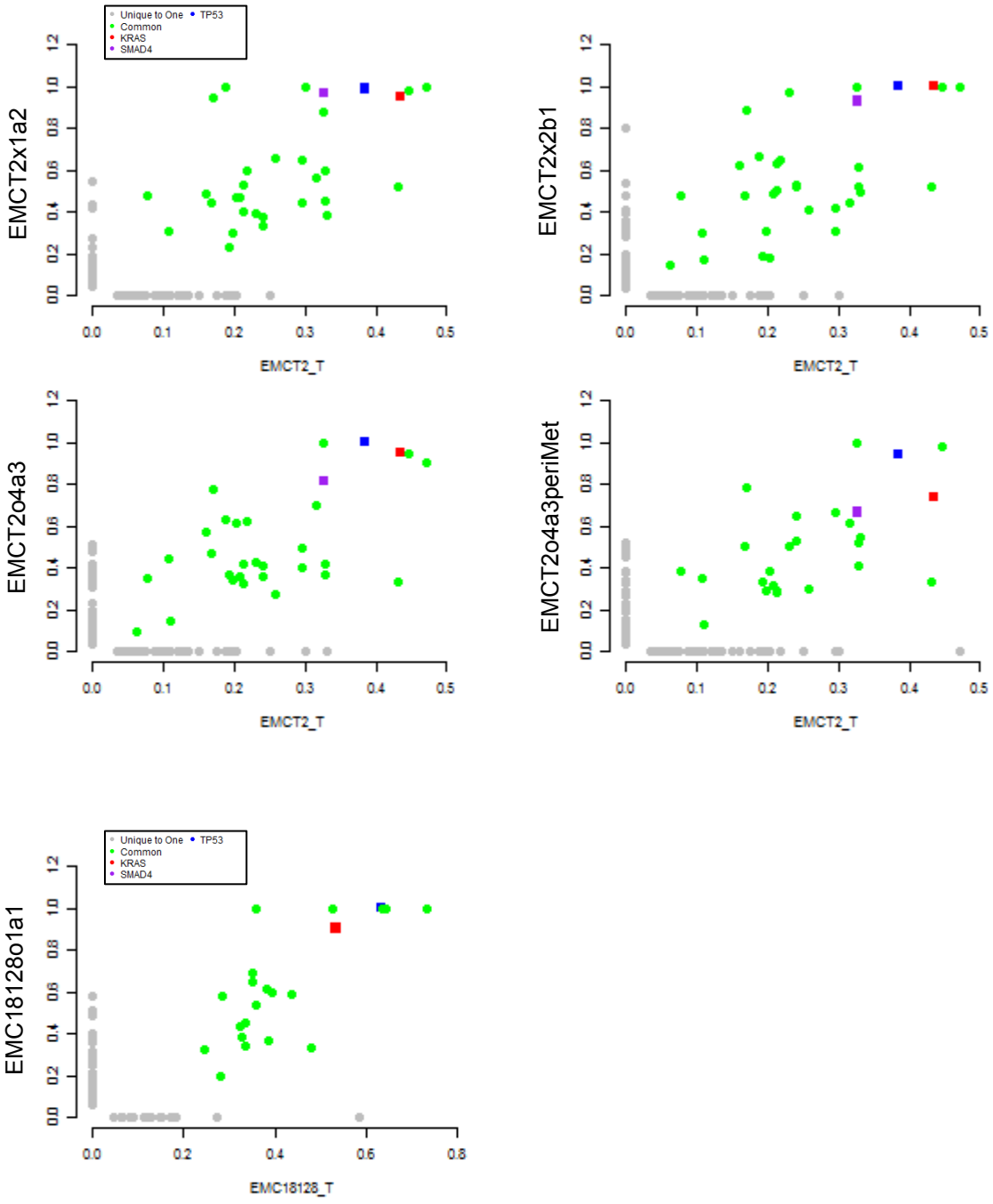
Unique to One
TP53
Common
KRAS
SMAD4
EMCT2x1a2
EMCT2x2b1
EMCT2o4a3
EMCT2o4a3periMet
EMC18128o1a1
EMCT2_T
EMC18128_T

C.

Tumor Case	Model SNV Summary (C=common, UC=unique to cell line, UT=unique to tumor)																																			
EMC26_T	X2b1_EP																																			
	C	UC	UT																																	
	16	13	6																																	
EMC514_T	514_EP																																			
	C	UC	UT																																	
	21	8	9																																	
EMC810_T	o1a1_EP																																			
	C	UC	UT																																	
	38	5	2																																	
EMC827_T	827_EP																																			
	C	UC	UT																																	
	38	26	8																																	
EMCT2_T	x1a2_EP			x2b1_LP																																
	C	UC	UT	C	UC	UT																														
	31	41	68	29	62	70																														
EMC2095_T	2095_EP			2095_LP																																
	C	UC	UT	C	UC	UT																														
	11	15	57	12	35	56																														
EMC7310_T	7310_EP			7310_LP																																
	C	UC	UT	C	UC	UT																														
	29	47	17	27	49	19																														
EMC18128_T	18128_EP			18128_LP																																
	C	UC	UT	C	UC	UT																														
	23	63	15	23	38	15																														
EMC29_T	o1a1_EP			o1a2_EP			o1a5 periMet_EP																														
	C	UC	UT	C	UC	UT	C	UC	UT																											
	31	13	32	31	12	32	30	12	33																											
EMC43_T	x1a1_LP			x1a2_EP			x1a2_LP																													
	C	UC	UT	C	UC	UT	C	UC	UT																											
	38	14	2	38	17	2	37	18	3																											
EMC519_T	519_EP			519_LP			x1a2_EP			x2a1_EP																											
	C	UC	UT	C	UC	UT	C	UC	UT	C	UC	UT																									
	16	3	2	16	9	2	16	6	2	16	7	1																								
EMC1229_T	1229_EP			1229_LP			x1a2_EP																													
	C	UC	UT	C	UC	UT	C	UC	UT																											
	5	30	19	5	30	19	6	46	18																											
EMC828_T	x1b1_EP			x1b3_EP			x2a3_EP			x2b2_EP			x3b1_EP																							
	C	UC	UT	C	UC	UT	C	UC	UT	C	UC	UT	C	UC	UT																					
	30	21	3	29	27	4	29	40	4	30	15	3	30	14	3																					
EMC226_T	226_EP			226_LP			x1a1_EP			x1a2_EP			o1a5_EP			o1a5met_EP																				
	C	UC	UT	C	UC	UT	C	UC	UT	C	UC	UT	C	UC	UT	C	UC	UT																		
	69	9	10	67	23	12	68	15	11	70	7	9	69	18	10	68	19	11																		
EMC1222_T	1222_EP			1222_LP			x1a3_EP			x1a3_LP			x1b1_EP			x3a1_EP			x3c2_EP			o2a1_EP			o2a1_LP			o2a2_EP						
	C	UC	UT	C	UC	UT	C	UC	UT	C	UC	UT	C	UC	UT	C	UC	UT	C	UC	UT	C	UC	UT	C	UC	UT	C	UC	UT					
	41	12	5	42	13	4	43	12	3	43	11	3	43	18	3	42	43	4	43	34	3	43	17	3	44	26	2	43	19	3					

D.

Cell Line

Mutant Allele Frequency Scatterplots

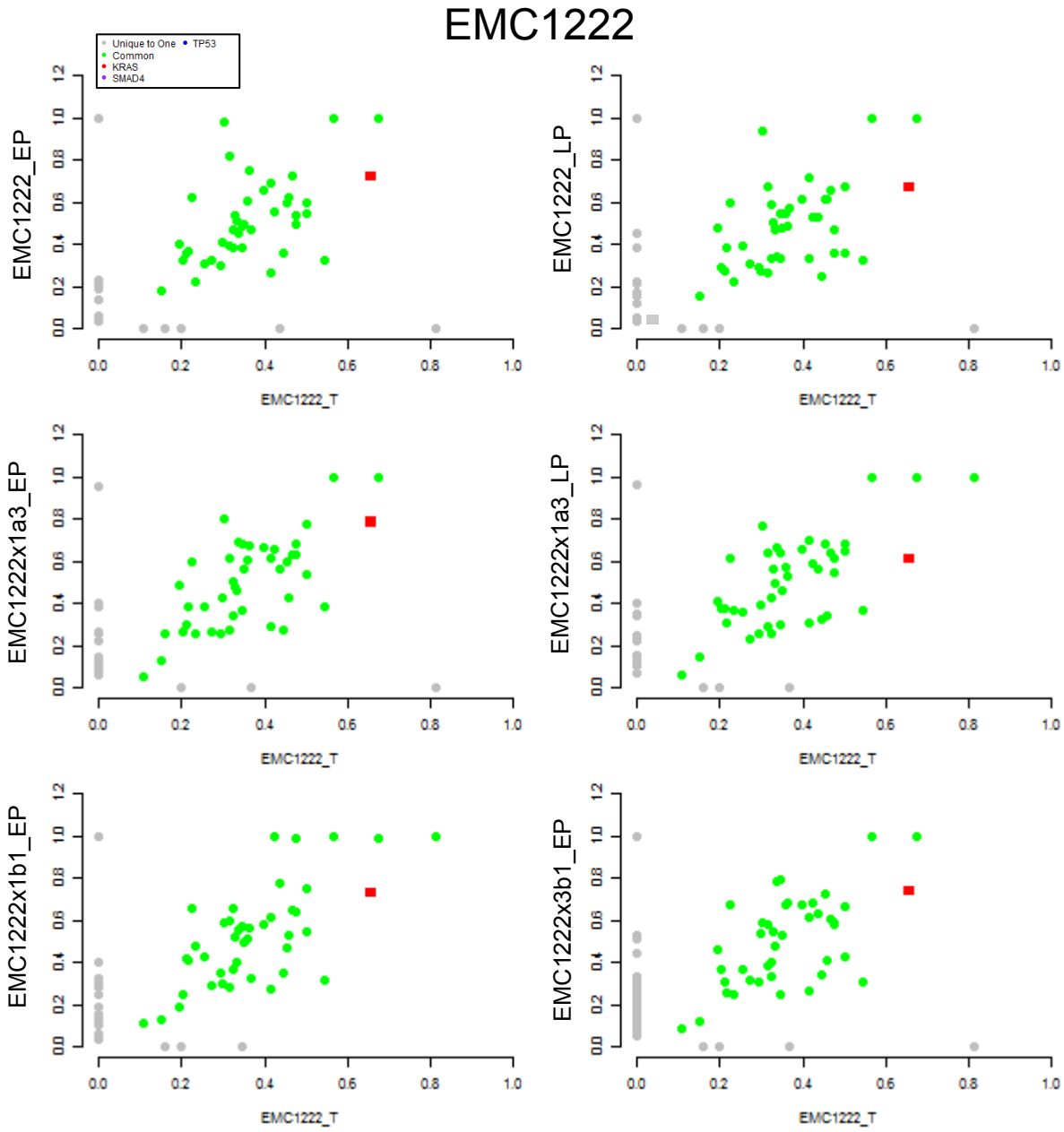

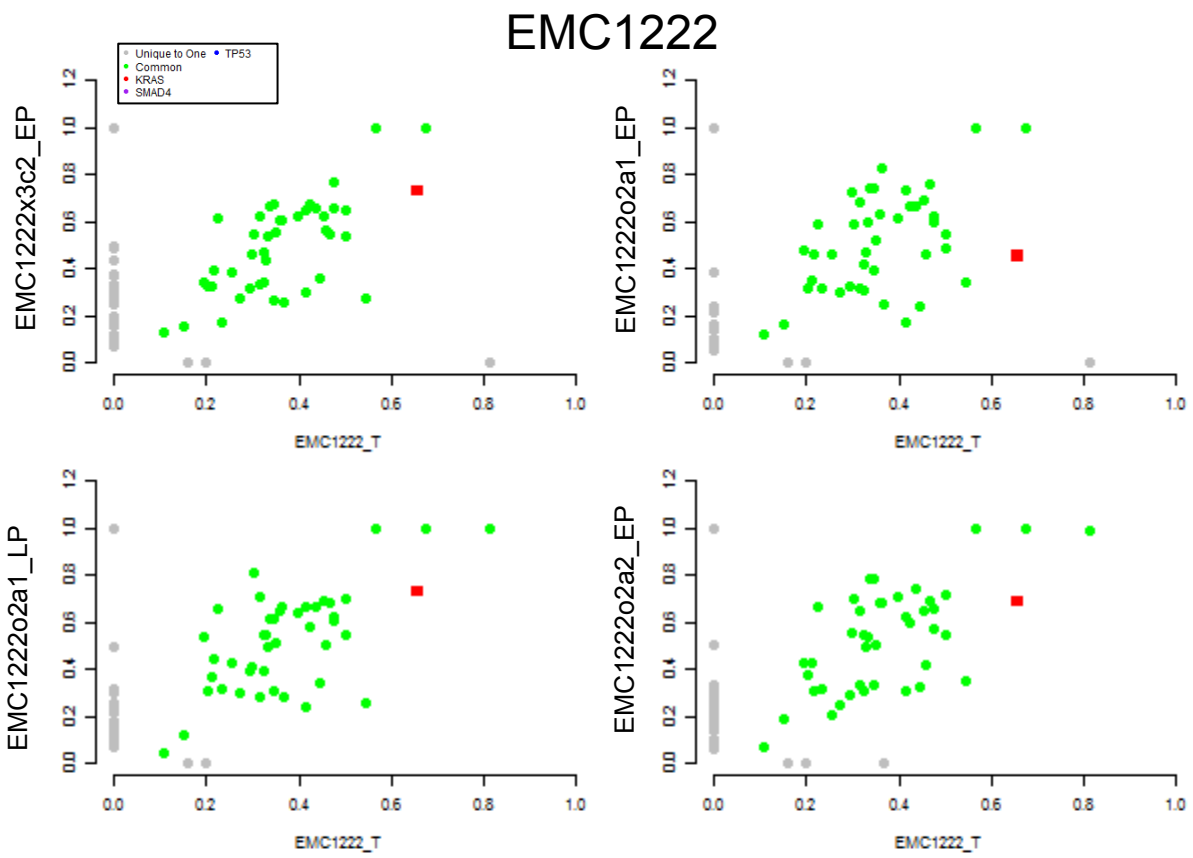
EMC1222
Unique to One
TP53
Common
KRAS
SMAD4
EMC1222x3c2_EP
EMC1222o2a1_EP
EMC1222o2a1_LP
EMC1222o2a2_EP
EMC1222_T
0.0
0.2
0.4
0.6
0.8
1.0
1.2

EMC226

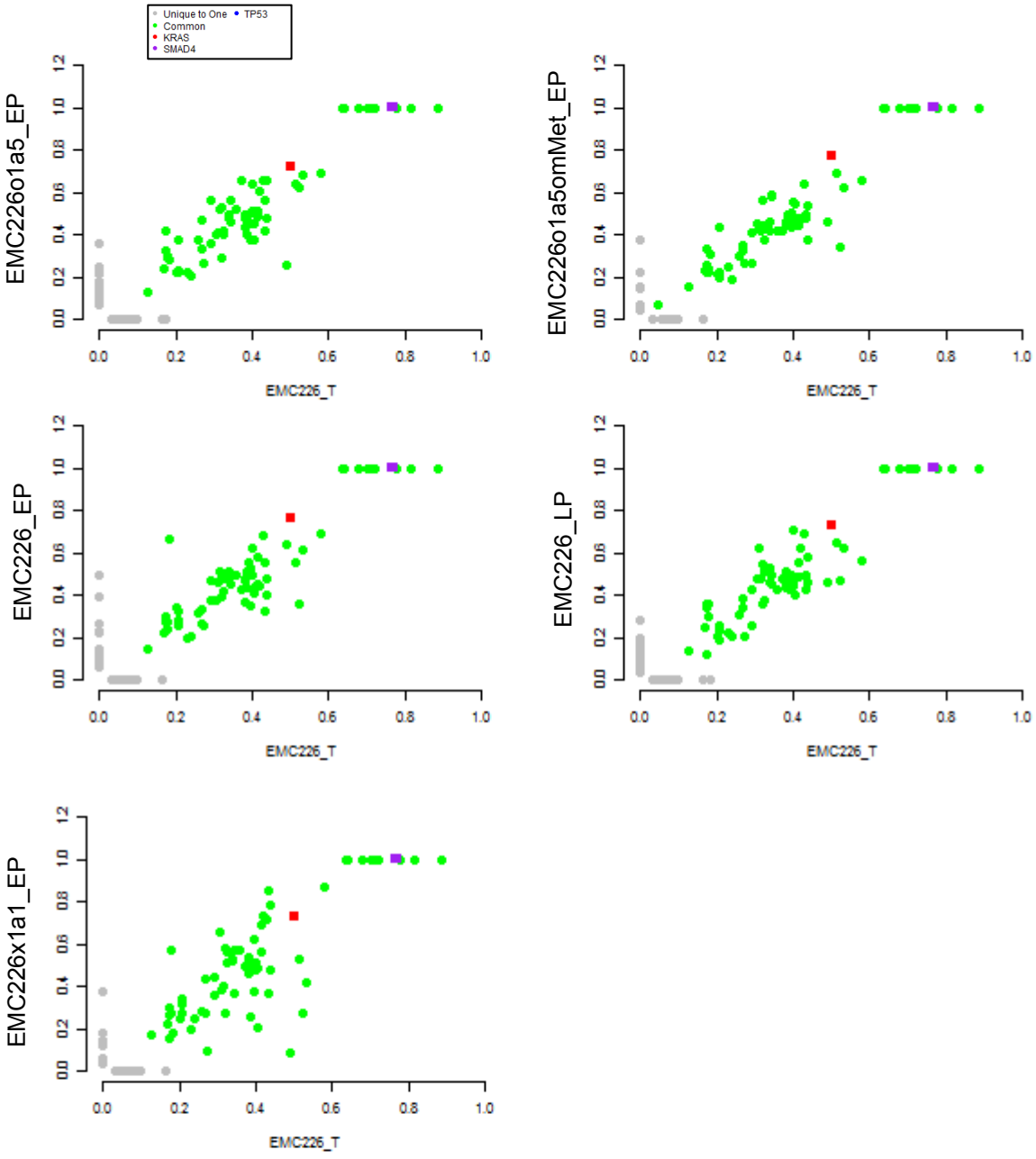
Unique to One
TP53
Common
KRAS
SMAD4
EMC226o1a5_EP
EMC226o1a5omMet_EP
EMC226_EP
EMC226_LP
EMC226x1a1_EP
EMC226_T
0.0
0.2
0.4
0.6
0.8
1.0
1.2

EMC828

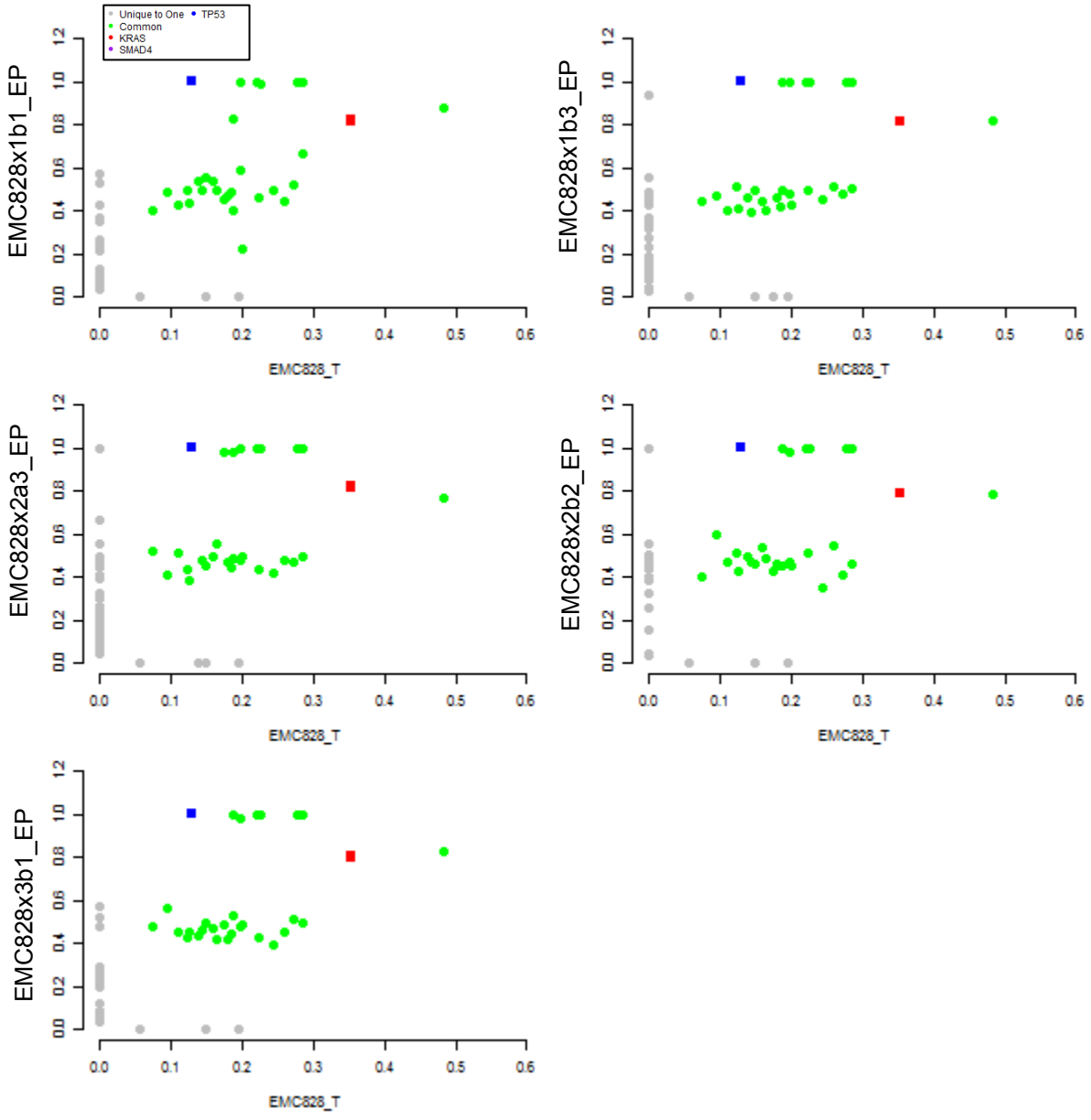
Unique to One
TP53
Common
KRAS
SMAD4
EMC828x1b1_EP
EMC828x1b3_EP
EMC828x2a3_EP
EMC828x2b2_EP
EMC828x3b1_EP
EMC828_T
0.0
0.2
0.4
0.6
0.8
1.0
1.2
0.1
0.3
0.5

EMC26

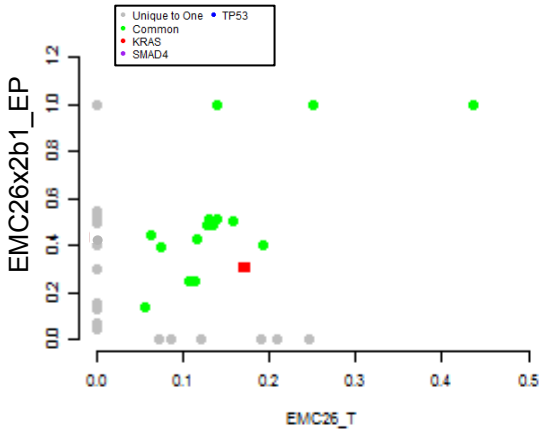
Unique to One
TP53
Common
KRAS
SMAD4
EMC26x2b1_EP
EMC26_T

EMC29

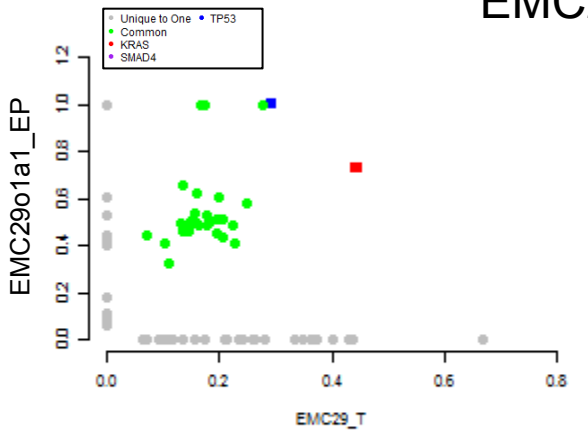
Unique to One
TP53
Common
KRAS
SMAD4
EMC29o1a1_EP
EMC29_T

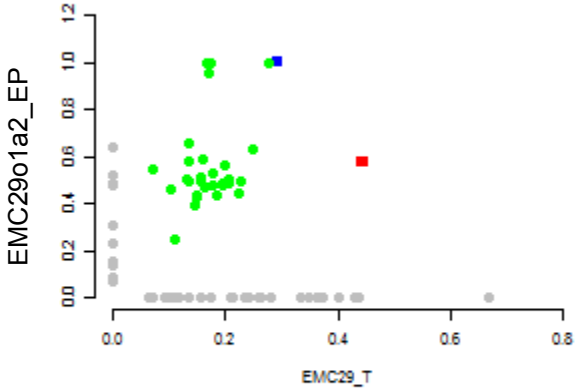
EMC29o1a2_EP
EMC29_T

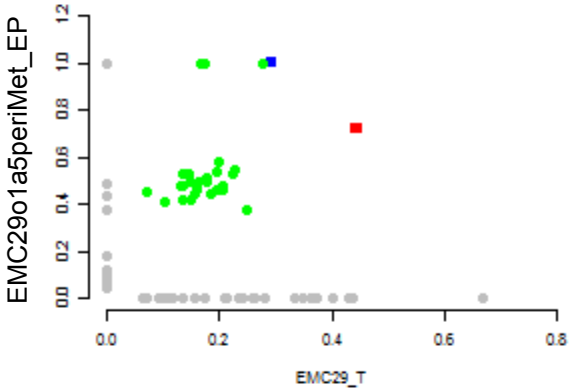
EMC29o1a5periMet_EP
EMC29_T

EMC43

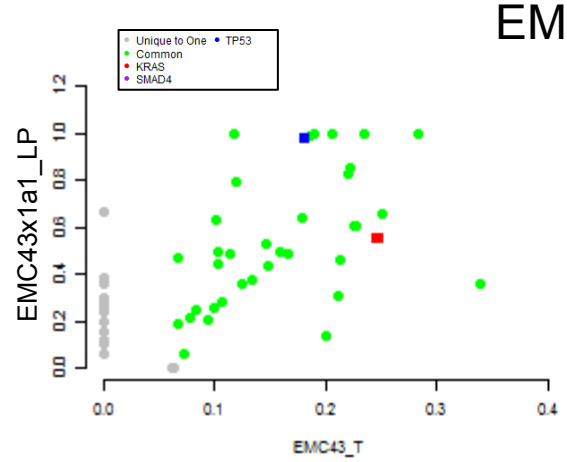

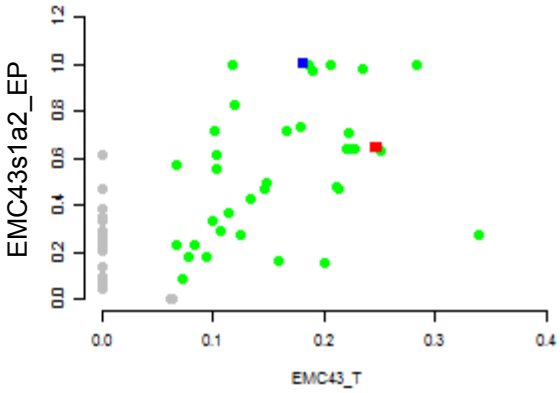

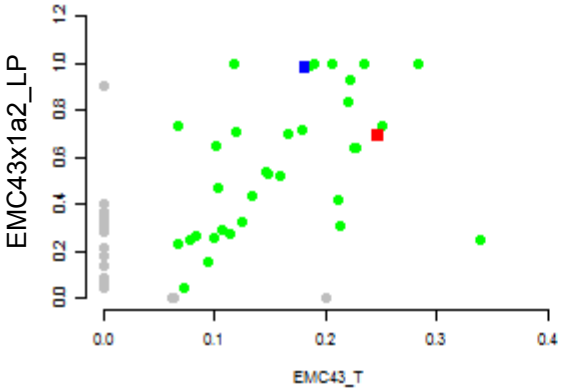

EMC514

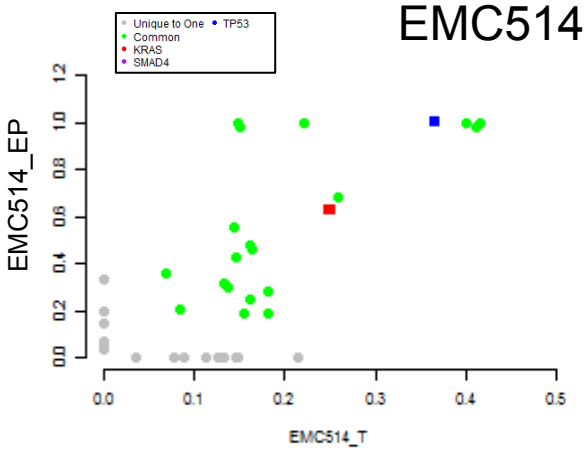

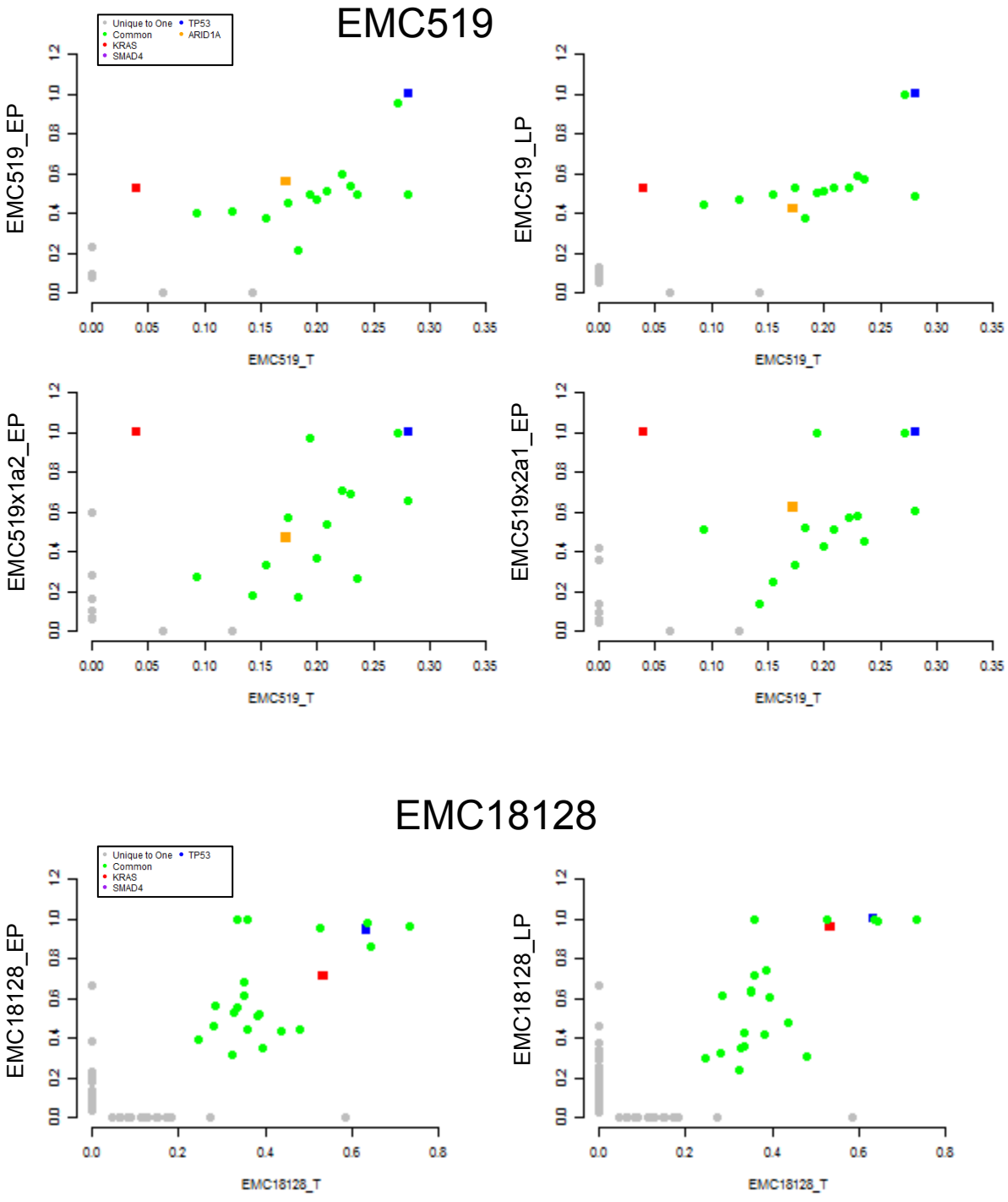
EMC519
Unique to One
Common
KRAS
SMAD4
TP53
ARID1A
EMC519_EP
EMC519_LP
EMC519x1a2_EP
EMC519x2a1_EP
EMC519_T
EMC18128
EMC18128_EP
EMC18128_LP
EMC18128_T

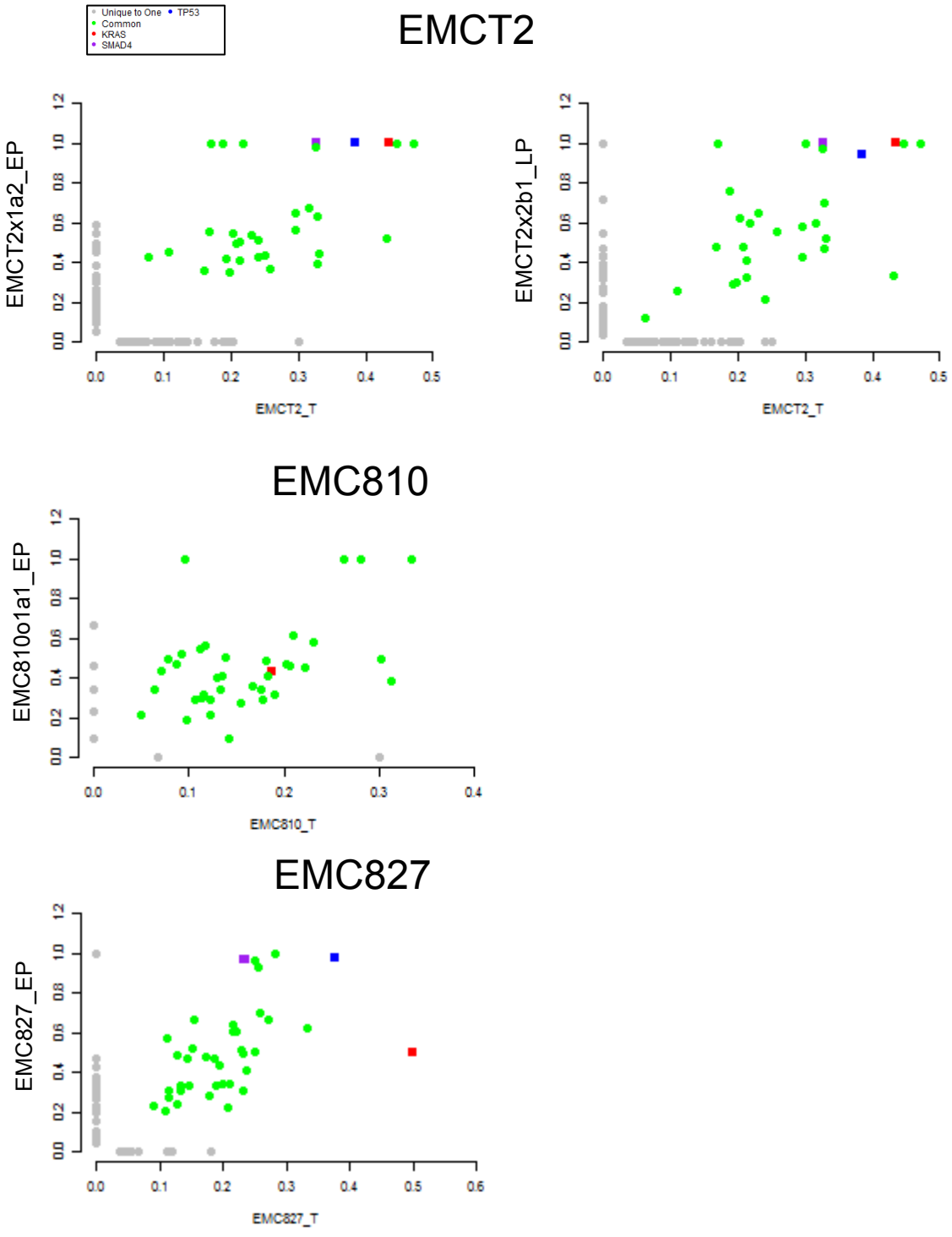
EMCT2
Unique to One
TP53
Common
KRAS
SMAD4
EMCT2x1a2_EP
EMCT2_T
EMCT2x2b1_LP
EMCT2_T
EMC810
EMC810o1a1_EP
EMC810_T
EMC827
EMC827_EP
EMC827_T

GO Term	p-value	Genes
transcription	8.61E-06	SCAF1, ZNF584, ZNF580, ZNF57, MED25, TBP, RORB, FOXO3, SOHLH1, BRPF1, MDFIC, ZNF248, FOXF2, FIZ1, ZNF575, EOMES, ZNF649, ARID1A, MED13, ZNF793, FOXN4, ZNF787, HIF1A, ZNF784, KDM2A, BAZ1B, PIAS3, PRDM6, ZNF239, TGIF1, ZNF383, HMX3, ZNF382, SUV420H1, ZNF613, CAMTA1, MYEF2, MYT1, ZNF616, ZNF699, ZNF229, MAML3, ASXL3, ZMYM2, TAF4, BHLHE22, SRA1, SMAD4, NEUROG1, SMYD1, NEUROG2, ESX1, ZNF836, ZNF628, ZNF837, NOTCH2, SALL2, NOTCH1, ZNF211, EBF3, HOXB5, ZNF418, ZNF17, ZNF83, ZNF534, POU6F2, ZNF530, NR6A1, ZNF155, ZNF12, ZNF674, ZNF345, ZNF678, MAZ, GTF2A1, ZNF148, NR2F6, KDM5A, TAF1L, ELP3, ZNF548, ZNF285, ZNF92, ZNF142, CDK8, ADNP, RUNX1T1, PADI4, IFI16, DMRTB1, MBD1, ZNF335, FAM120B, HIPK3, ZNF717, ZNF551, SRCAP, ZFP62, BCLAF1, ZNF469, ZNF274, ZNF552, ZNF468, ZNF557, ZBTB9, BDP1, CTNND2, IVNS1ABP, TCF7L1, CHD8, PER1, ZNF286A, CHD5, ERCC2, ZNF267, JARID2, POLR3A, MEF2D, ATXN3, DACH2, PHF21A, ZNF462, TCEB1, ZNF765, PBX2, MESP2
cell differentiation	3.20E-04	FGF5, NEURL, HRNR, POU6F2, DICER1, OSGIN1, RORB, GRIN3A, FOXO3, TTN, PRKG1, SOHLH1, WNT2, AKT1, DSPP, GSN, SEMA3D, NR2F6, POU4F2, CDK5RAP2, SIK1, IHH, TCHH, SRPK2, CTBP1, CTBP2, MDGA1, KIF5C, EOMES, STXBP1, RUNX1T1, IFI16, MYH9, SLIT1, MARK2, FOXN4, NUMBL, DCLRE1C, SLITRK1, HIF1A, TXNDC2, FAM120B, PRDM6, SPRR3, TGIF1, ROR2, COL1A1, LAMC1, HMX3, KALRN, CALCR, PARD3, BLM, PTH1R, MYEF2, TRIM15, MYT1, SCRIB, TCF7L1, SPEG, DGKG, UPK1A, AGT, PVRL2, ZAP70, OBSL1, KRT2, KRT4, RASA1, ERCC2, APC, ACTB, IL4, DFNA5, BHLHE22, SRA1, SMAD4, NEUROG1, NEUROG2, DOCK7, INSC, CAPN3, NTRK3, NOTCH2, MEF2D, NOTCH1, LAMA4, COL19A1, FLG, LCE1F, CDON, HOXB5, GDF11, AMOT, JAK2, MYH10

A.

QM (n=23) vs. Other (n=33)	
CompundID	pvalue
Dasatinib (BMS-354825)	0.000297
OSI-420	0.000312
Erlotinib HCl	0.000454
AG-1478 (Tyrphostin AG-1478)	0.001389
PD153035 HCl	0.002823
AZD8931	0.004022
PHA-767491	0.005143
Desmethyl Erlotinib (CP-473420)	0.009616
AST-1306	0.010458
Dacomitinib (PF299804,PF-00299804)	0.011639
CI-1033 (Canertinib)	0.01383
Afatinib (BIBW2992)	0.015351
YM201636	0.015886
Wortmannin	0.01661
Acadesine	0.019666
BIRB 796 (Doramapimod)	0.020014
Hesperadin	0.023097
Gefitinib (Iressa)	0.028199
AEE788 (NVP-AEE788)	0.029014
AG-490	0.03533
A-674563	0.041054
Vorinostat (SAHA)	0.042107
MLN8054	0.042267
Ponatinib (AP24534)	0.043184
WYE-687	0.045003
MK-8245	0.046376

Established Cell Lines (n=9) vs QM (n=23) or Other (n=33)		
CompundID	pvalue (QM)	pvalue (other)
AST-1306	1.28342E-05	1.76955E-11
ABT-737	3.83352E-06	4.87392E-11
Tyrphostin AG 879 (AG 879)	0.000457605	3.44009E-06
GSK1059615	0.000173766	3.97196E-06
Entinostat (MS-275, SNDX-275)	0.001585876	1.1246E-05
CI-1033 (Canertinib)	0.016005386	2.58104E-05
Erlotinib HCl	0.038891624	4.64621E-05
PIK-293	0.001417672	4.79681E-05
Quercetin (Sophoretin)	0.000127844	5.06752E-05
R788 (Fostamatinib)	0.000394408	6.21242E-05
AG-1478 (Tyrphostin AG-1478)	0.153623947	8.12516E-05
WZ3146	0.020835405	9.36661E-05
XL147	0.001921775	0.000116667
Wortmannin	0.005811691	0.000121996
R406	0.000139694	0.0001319
AG-1024	0.00088721	0.000219391
Milciclib (PHA-848125)	0.001633767	0.000245704
Docetaxel (Taxotere)	0.000477978	0.000301273
WP1066	0.020341646	0.000331493
PCI-32765 (Ibrutinib)	0.03131531	0.000354023
NVP-TAE226	0.000797685	0.000427499
Paclitaxel (Taxol)	0.000321744	0.000471469
OSI-420	0.057397361	0.000477759

B.